Economic Geology, v. 113, no. 8, pp. 1817–1843

How Precisely Can the Temperature of a Fluid Event be Constrained Using Fluid Inclusions?

András Fall[1,†] and Robert J. Bodnar[2]

[1] *Bureau of Economic Geology, Jackson School of Geosciences, The University of Texas at Austin, Austin, Texas 78713*

[2] *Fluids Research Laboratory, Department of Geosciences, Virginia Tech, Blacksburg, Virginia 24061*

Abstract

Fluid inclusions in clearly defined fluid inclusion assemblages (FIAs) from various geologic environments were examined to assess the uncertainty associated with determining the temperature of a fluid event based on fluid inclusion homogenization temperatures (T_h). A fluid event is defined as a physical or chemical process such as the healing of a microfracture or the formation of a growth zone in a crystal that occurs in the presence of a fluid phase and results in trapping of fluid inclusions to form an FIA. Examination of data from a large number of fluid events collected within a rigorous temporal and spatial (paragenetic) framework forms the basis for developing a complete fluid pressure-temperature-composition (PTX) history.

The range in homogenization temperatures of fluid inclusions within well-constrained FIAs was determined, and the minimum (smallest) range in T_h, the median range in T_h, and the first quartile (Q1 at 25%) and third quartile (Q3 at 75%) of the median T_h ranges were calculated for different fluid environments, including the following:

1. Low-permeability sedimentary environments: 49 out of 144 FIAs show a range in T_h of ≤1°C; the median range = 2°C (from Q1 = 1°C to Q3 = 3.7°C).
2. Mississippi Valley-type deposits: 11 out of 137 FIAs show a range in T_h of ≤1°C; the median range = 4.1°C (from Q1 = 2.3°C to Q3 = 8.3°C).
3. Epithermal deposits: 102 out of 923 FIAs show a range in T_h of ≤1°C; the median range = 9°C (from Q1 = 3.8°C to Q3 = 19°C).
4. Porphyry-type deposits: 24 out of 271 FIAs show a range in T_h of ≤ 1°C; the median range = 15°C (from Q1 = 8°C to Q3 = 30°C).
5. Orogenic Au deposits: 21 out of 231 FIAs show a range in T_h of ≤1°C; the median range = 8.7°C (from Q1 = 4°C to Q3 = 20°C).

While all environments show some FIAs in which all the fluid inclusions homogenize at essentially the same temperature (range = ≤1°C), we propose that the median range in T_h reported here represents a reasonable and achievable constraint on the uncertainty associated with the temperature of a fluid event in the environments examined. In summary, the temperature of a fluid event, as represented by the range in T_h of the fluid inclusions within an individual FIA, can be constrained to better than 15°C in all environments examined, and in Mississippi Valley-type and low-permeability (deep) sedimentary basin environments, the range in T_h can be constrained to better than 2°C.

The processes that produce variability in T_h of fluid inclusions within an FIA are many and include natural variations in temperature, pressure, or fluid composition during trapping of the FIA, trapping of immiscible fluids, various forms of reequilibration in nature such as necking, stretching, and leakage, and modification of the inclusions during sample preparation and data collection. If the range in homogenization temperature for an individual FIA is found to be greater than the median range determined here for that environment, then assessment of the cause of the variability might provide useful information concerning the trapping and post-trapping history of the sample.

Introduction

Thermometric data obtained from fluid inclusions is a standard tool for constraining the pressure-temperature-composition (PTX) history of fluids associated with geologic processes spanning the sedimentary to metamorphic to igneous environments (Roedder, 1984). Although a rigorous methodology for the collection of fluid inclusion data has been developed over the years (Touret, 1981; Roedder, 1984; Diamond, 1990; Goldstein and Reynolds, 1994; Fonarev et al., 1998; Van den Kerkhof and Hein, 2001; Bodnar, 2003a; Goldstein, 2003), acceptable or achievable ranges in microthermometric data for groups of coeval fluid inclusions have not been rigorously evaluated and defined. The goal of this study is to determine ranges in homogenization temperature (T_h) for well-characterized fluid inclusion assemblages (FIAs) from various geologic environments in an attempt to provide guidance concerning the achievable range in T_h.

The most important requirement in a fluid inclusion study is to collect data that are related to the question or problem being addressed. Moreover, data should be collected following a protocol that allows one to place data into a temporal and spatial context and to assess the quality of the data. The FIA framework (Goldstein and Reynolds, 1994) meets these requirements and allows one to test whether the fluid inclusions

† Corresponding author: e-mail, andras.fall@beg.utexas.edu

ISSN 0361-0128; doi: 10.5382/econgeo.2018.4614; 27 p.
Supplementary file available online.

Submitted: July 13, 2018
Accepted: November 6, 2018

record the original trapping conditions or have been modified after trapping. The requirements necessary for fluid inclusions to provide a record of the physical and chemical environment at the time of trapping are often referred to as "Roedder's rules" and include the following:

1. The fluid inclusion traps a single, homogeneous phase.
2. The fluid inclusion volume remains constant after trapping (i.e., isochoric).
3. Nothing is lost from, or added to, the fluid inclusion after trapping.

Fluid inclusion assemblages are defined as the most finely discriminated, petrographically associated group of coeval inclusions (Diamond, 1990; Goldstein and Reynolds, 1994; Bodnar, 2003a). In many cases, an FIA is manifest as a group of fluid inclusions decorating a healed or sealed fracture or outlining a growth surface in a crystal. Implicit in the FIA definition is that all of the fluid inclusions within the FIA were trapped at (essentially) the same time, and this can be extended to infer that all of the fluid inclusions in the FIA were trapped at the same temperature and pressure and that all trapped a fluid of the same composition. It follows then that all of the fluid inclusions within the FIA should contain the same number of phases and in the same volume proportions when observed at room temperature, and all of the fluid inclusions in the FIA should display similar behavior during microthermometry. This assumes, of course, that the fluid inclusions within the FIA were trapped over a relatively short (but undefined) period of time such that the pressure-temperature conditions remained constant. However, some FIAs may consist of primary fluid inclusions contained within a relatively thick growth band lacking internal zonation. Such fluid inclusions may show systematic temperature variations with respect to their location in the growth band, suggesting that the temperature and/or pressure varied during formation of the growth band (see Goldstein and Reynolds, 1994, fig. 7.1). By extension, all of the primary fluid inclusions contained within a single crystal that lacks zonation may be considered to represent a single FIA, because all of the inclusions were trapped during growth of the crystal, and that event (growth of the entire crystal) is the most finely discriminated association that is possible. Of course, the crystal could have formed over a considerable period of time, and the formation conditions might have varied significantly during formation of the crystal and its contained fluid inclusions. Similarly, heterogeneous trapping and various post-trapping processes can lead to variability in the phase proportions and microthermometric behavior of the fluid inclusions within an FIA, as described in more detail below.

Although much work has been done to understand the precision and accuracy with which the T_h (and other microthermometric data) of an individual fluid inclusion can be determined (Hollister et al., 1981; Roedder, 1984), our understanding of the acceptable ranges in T_h for FIAs in various geologic environments is poor. A goal of this study, therefore, is to determine ranges in T_h for well-characterized FIAs in order to provide a basis for assessing the range in T_h that characterizes a fluid event in different geologic environments, which may, in turn, be used to evaluate the reliability of the inclusions as recorders of the PTX history of trapping. Stated simply, how precisely can the temperature of a fluid event be constrained using fluid inclusions? Here, we use the term "fluid event" to indicate an event such as the healing of a fracture or formation of a growth zone in a crystal, with the concomitant trapping of fluid inclusions in the process. It should also be emphasized that in this study we report only T_h, recognizing that the actual trapping temperatures will be somewhat higher, except for those inclusions trapped from immiscible fluids. And, because all isochores diverge (fan out) at higher pressure, the range in temperature of formation or trapping of an FIA will always be greater than the observed range in T_h for that same FIA.

Methods

Sample preparation and microthermometry

The samples used in this study represent previously well documented magmatic, metamorphic, hydrothermal, and sedimentary environments. All samples contain well-constrained FIAs, and in most cases the FIAs could be placed into a rigorous paragenetic (temporal) framework. That is, the FIAs could be related to a specific event (i.e., growth zone or mineralization stage), but the relative ages of FIAs within each growth zone or stage were often poorly constrained. Doubly polished thick sections were prepared from each sample with care to exclude mechanical or thermal damage to the inclusions during preparation.

FIAs are defined based only on petrographic features. In many cases it was necessary to examine several polished sections prepared from a single sample or environment to identify well-constrained FIAs along crystal growth zones (i.e., Fig. 1a-c, e-f), in 3-D clusters or the cores of crystals (Fig. 1d), or in healed microfractures (Fig. 2a-c, e-f). In some samples, FIAs were easily recognized, because the host phase was transparent and contained relatively few inclusions along either well-defined growth zones or fractures, or both. Other samples showed so many fluid inclusions within a field of view or small area of the polished section that individual FIAs could not be unambiguously defined. For such samples, individual FIAs could sometimes be distinguished if the section was made thinner to reduce the abundance of fluid inclusions in the field of view. In the present study, the initial thick sections were prepared to about 1-mm thickness. At this thickness it was often possible to identify individual FIAs in fluorite from the Cave-in-Rock district, which contains relatively few, large fluid inclusions. However, in similarly thick samples from other environments, the opacity of the host caused by the abundance of fluid inclusions precluded the identification of FIAs. Such samples were further thinned and monitored under the microscope until individual FIAs could be clearly identified. In cases where this strategy did not allow individual FIAs to be identified with confidence, the sample (polished section) was eliminated from further study. After FIAs were identified, the glass slide was cut into small pieces that contained one or a few FIAs to be measured, with the doubly polished section still attached to the slide. Then, the doubly polished chip was removed from the glass slide by dissolving the cement in acetone before microthermometry. Data were collected during the first and only heating run on any individual FIA. This method prevented overheating of the inclusions that could lead to stretching or leakage and result in a T_h higher than the original or true T_h (Goldstein and Reynolds, 1994; Bodnar, 2003b).

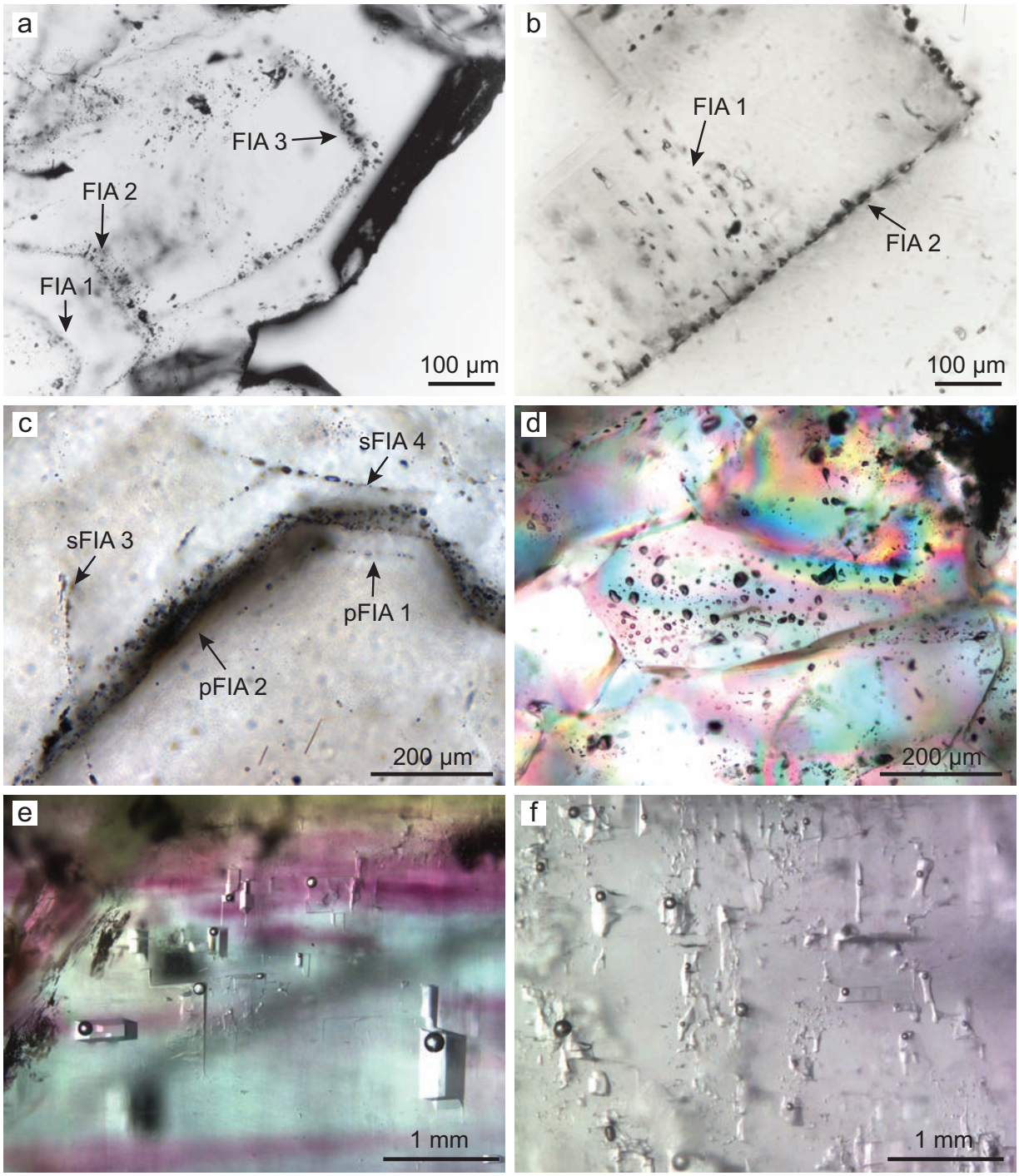

Fig. 1. Examples of fluid inclusion assemblages (FIAs) containing primary fluid inclusions. (a) Photomicrograph of a portion of a quartz crystal from the epithermal Ag deposits at Guanajuato, Mexico, showing three primary FIAs outlining former growth surfaces in the crystal. (b) Photomicrograph of a portion of a quartz crystal from the epithermal Ag deposits at Guanajuato, Mexico, showing two FIAs: one (FIA 1) contained within a growth band in the crystal and the other (FIA 2) outlining the growth surface that terminates the growth band. These two FIAs likely represent one fluid event associated with growth of the quartz crystal. (c) Photomicrograph of a portion of a quartz vein from the Copper Creek, Arizona, porphyry prospect showing two FIAs (pFIA 1 and pFIA 2) containing primary inclusions along growth surfaces in the crystal and two FIAs (sFIA 3 and sFIA 4) containing secondary inclusions trapped along healed fractures in the quartz. (d) Photomicrograph of a portion of a quartz vein from the Marte porphyry-epithermal system, Chile, showing an FIA consisting of vapor-rich fluid inclusions. (e) Photomicrograph of a portion of a fluorite crystal from the Cave-in-Rock district, southern Illinois, showing an FIA consisting of primary, negative crystal-shaped inclusions that are contained within a single color-banded growth zone in the fluorite crystal. (f) Photomicrograph of a portion of a fluorite crystal from the Cave-in-Rock district, southern Illinois, showing an FIA consisting of primary, irregularly shaped inclusions that are all contained within a single growth band in the fluorite. Note that even though the inclusions are mostly irregularly shaped, they all homogenize at the same temperature (±1°C).

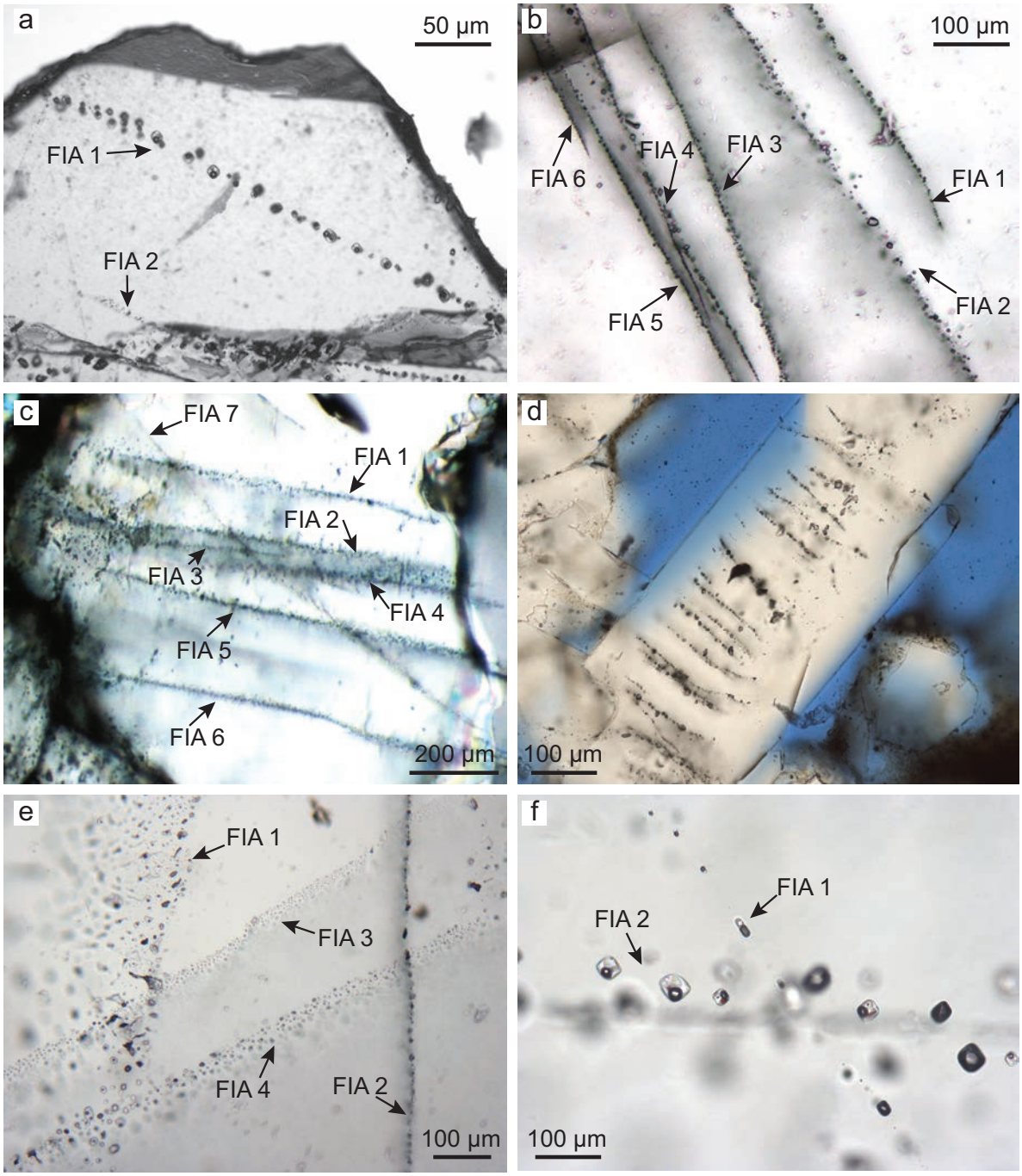

Fig. 2. Examples of fluid inclusion assemblages (FIAs) containing secondary fluid inclusions. (a) Photomicrograph of a portion of a quartz vein from the Copper Creek, Arizona, porphyry prospect showing two healed fractures (FIA 1 and FIA 2) containing secondary fluid inclusions. (b) Photomicrograph of a portion of a quartz vein from the North American Emerald mine, North Carolina, showing six healed fractures containing secondary fluid inclusions. Each healed fracture represents a different FIA, although all six of these FIAs likely formed at the same time or during the same fracturing and healing event. (c) Photomicrograph of a portion of a quartz vein from the Morro Velho gold deposit, Brazil, showing numerous healed fractures containing secondary FIAs. Note that under reflected light small (1–2 μm) gold grains can be seen along these healed fractures containing secondary fluid inclusions, suggesting that the secondary fluid inclusions on the fractures represent the inclusions one should study to determine the fluid conditions associated with gold mineralization. (d) Numerous FIAs in a quartz fracture cement bridge from the Piceance basin, Colorado, containing pseudosecondary fluid inclusions. Note that the trails terminate within the crystal due to continuous growth of the quartz after fracturing ceased (see Fall et al., 2015, for more details). (e) Photomicrograph of a portion of a fluorite crystal from the Cave-in-Rock district, southern Illinois, showing several healed fractures containing secondary fluid inclusions. Each healed fracture represents a separate FIA, although some of the FIAs, especially those with similar orientations, may have formed contemporaneously during the same fracturing and healing event. (f) Photomicrograph of a portion of a quartz vein from the Copper Creek, Arizona, porphyry prospect showing two crosscutting healed fractures, each representing a different FIA.

Microthermometric analyses were conducted using a FLUID INC.-adapted U.S. Geological Survey (USGS) gas-flow heating/freezing stage (Werre et al., 1979) mounted on an Olympus BX 51 microscope equipped with a 40× objective (N.A. = 0.55) and 10× oculars. The gas-flow stage was preferred in this study because of the ease with which the temperature could be cycled to facilitate determination of the T_h in smaller and/or irregularly shaped inclusions in which the bubble could not be easily observed as T_h is approached. The stage was calibrated using the CO_2-ice melting temperature at –56.6°C of H_2O-CO_2 synthetic fluid inclusions, and the ice-melting temperatures at 0°C and critical T_h at 374.1°C of pure H_2O synthetic fluid inclusion standards (Sterner and Bodnar, 1984). Liquid-vapor T_h were determined with a precision of ±0.05°C. For some fluid inclusions the thermal cycling technique was used to bracket T_h when it was difficult to observe the final disappearance of the vapor bubble during continuous heating (Goldstein and Reynolds, 1994).

Data presentation

Microthermometric data from fluid inclusions are often plotted on histograms. While histograms show the complete range in T_h and salinity in the system being studied, such plots provide little or no information concerning the temporal evolution in temperature and salinity of the hydrothermal fluid. However, if the fluid inclusion data are collected within a well-defined mineral and fluid inclusion paragenetic framework, much more information is potentially available concerning the evolution of temperature, pressure, and fluid salinity during inclusion formation.

An example of the more in-depth understanding that is gained by collecting and displaying fluid inclusion data within a rigorous FIA and paragenetic framework is provided by data from a large, chemically and color-zoned sphalerite crystal (Fig. 3a) from the OH vein of the Creede, Colorado, epithermal Zn-Ag-Pb deposit (Roedder, 1974; Woods et al., 1982). Homogenization temperature and salinity data obtained from fluid inclusions in this sample are plotted as histograms in Figure 3b and c, respectively. The histograms show that T_h ranges from about 200° to 270°C, with an average at 240°C, and salinity ranges from about 5 to 11 wt % NaCl equiv, with an average around 8.5 wt % NaCl equiv (Table 1). Based on the data in the histograms, the complete ranges in temperature and salinity during formation of the sphalerite crystal are known, but how these parameters varied during crystal growth cannot be inferred from the histograms. However, the microthermometric data shown in Figure 3b and c were obtained from 20 FIAs that were identified based on their location within individual color (growth) bands of the crystal (Fig. 3a), thus establishing a stratigraphic succession and the relative ages of the different FIAs in the crystal. If the data are plotted on a salinity versus T_h diagram and the relative ages of the individual FIAs are labeled (Fig. 3d), the results reveal a complex history of fluid evolution during mineralization.

The same microthermometric data for the Creede sphalerite shown in Figure 3 have been replotted on Figure 4, showing the evolution in T_h (Fig. 4a) and salinity (Fig. 4b), both as a function of FIA number, with FIA 1 the oldest and FIA 20 the youngest. As shown, the decrease in both temperature and salinity between FIAs 1 and 2 (Fig. 4) could be interpreted to represent the influx of cooler, lower-salinity meteoric water into the hydrothermal system. Similarly, the increase in temperature and salinity during trapping of FIAs 6 through 8 (Fig.

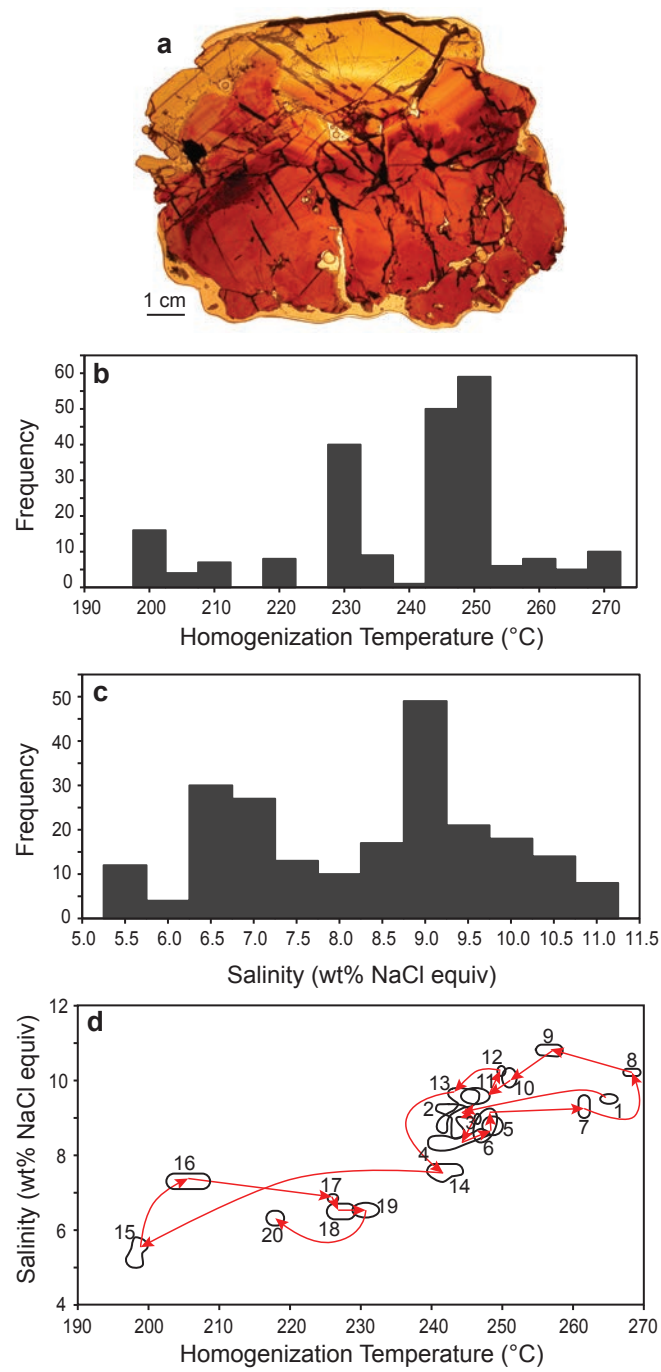

Fig. 3. (a) Large, color-zoned sphalerite crystal from the OH vein of the Creede epithermal Ag-Pb-Zn deposit, Colorado. (b) Histogram showing homogenization temperatures of fluid inclusions in the crystal shown in (a) (data from Roedder, 1974). (c) Histogram showing salinities of fluid inclusions in the crystal shown in (a) (data from Roedder, 1974). (d) The same homogenization temperature and salinity data that are shown in (b) and (c) plotted in salinity versus homogenization temperature space, with the relative ages of the different fluid inclusion assemblages indicated; 1 is the oldest and 20 is the youngest.

Table 1. Average Homogenization Temperatures (T_h), Range in T_h, and Salinity of Individual FIAs in Sphalerite from the Creede, Colorado, Epithermal Ag-Zn-Pb Deposit (data from Roedder, 1974)

FIA	No. of inclusions in the FIA	Average T_h (°C)	ΔT_h (°C)	Salinity (wt % NaCl equiv)
1	2	264.9	1.2	9.5
2	18	243.1	2.9	9.0
3	1	246.5	0.0	9.0
4	21	242.6	6.3	8.5
5	27	247.7	2.0	8.8
6	9	247.0	2.0	8.8
7	4	261.6	0.6	9.3
8	9	268.1	1.5	10.2
9	8	256.3	2.0	10.8
10	4	250.9	0.9	10.1
11	15	246.6	2.6	9.5
12	2	250.4	0.0	10.2
13	7	243.0	4.0	9.1
14	12	241.3	3.4	7.6
15	16	198.3	1.1	5.4
16	11	205.6	4.3	7.3
17	4	225.7	2.2	6.8
18	32	227.4	3.2	6.5
19	13	230.5	1.4	6.5
20	8	217.9	1.2	6.3

FIA = fluid inclusion assemblage

4) might indicate a new pulse of higher-temperature, higher-salinity magmatic-hydrothermal fluid into the system, and the significant decrease in both temperature and salinity associated with FIAs 14 and 15 (Fig. 4) might represent collapse of the meteoric water system late in the history of the magmatic-hydrothermal system. These processes that are inferred from the fluid evolution shown in Figure 4 could then be further investigated by comparison with other samples and by using additional geochemical data, such as variations in stable isotopic composition, which might confirm the relative proportions of magmatic versus meteoric water during the different stages of sphalerite growth represented by the FIAs.

In this study, T_h of individual FIAs are displayed as box and whisker plots. Thus, on Figure 4, primary fluid inclusions in each growth zone represent an FIA, and all of the data (T_h and salinity) for each of the 20 FIAs are plotted. The bottom and top of the colored boxes represent the 25th and 75th percentiles, respectively, and the horizontal line within the box represents the median value. The box and whiskers method and similar methods of displaying fluid inclusion data have been used previously to show T_h (e.g., Eichhubl and Boles, 2000; Landtwing et al., 2010; Marshall et al., 2016) and salinity variations (e.g., Landtwing et al., 2010; Pelch et al., 2015; Marshall et al., 2016), but this method of illustrating fluid inclusion data is used with far less frequency than histograms or T_h salinity plots. For each of the environments investigated, the median range and the first (25%) and third (75%) quartiles of the range in T_h of all FIAs were calculated (Electronic App. Table A1).

We note that the manner in which fluid inclusion data are displayed and distributed depends on the type of study being conducted and the questions being asked. If fluid inclusions are being used in an active exploration project where one needs only to know the approximate temperature and requires the information quickly, one can conduct a heating run to determine if all the fluid inclusions in the FIA show similar behavior, record that temperature, and immediately report this value to the client verbally or via electronic means without the need to develop detailed plots of the data as described above. In some cases, temperatures may not be needed at all—for example, if one is applying fluid inclusions in exploration for epithermal precious metal deposits and wants only to know if the fluids were boiling at the location where the sample was collected (cf. Moncada et al., 2017), this can be determined from petrography alone without the need for microthermometry. The box and whiskers method for displaying data described above is recommended if one is conducting a study to determine the physical and chemical conditions associated with formation of a mineral deposit or hydrocarbon reservoir and is developing a detailed fluid and thermal history of the deposit or reservoir in both time and space. Thus, the protocol described here does not apply to all fluid inclusion studies, depending on the nature of the study being conducted and the goals of that study.

Results—Ranges in Homogenization Temperatures Within Fluid Inclusion Assemblages

In order to determine ranges in T_h within an FIA that one might expect in different geologic environments, we collected data from samples from sedimentary basins, metamorphic environments, and magmatic-hydrothermal systems. Additional data from the literature that were collected within a strict FIA framework were combined with the data obtained in this study to expand the database. Ranges in T_h data for each environment from this study and from the literature are summarized in Table 2, and all FIAs from all environments that were included in our assessment are presented in Electronic Appendix Table A1.

Piceance basin, Colorado: Tight-gas sandstone reservoirs, hydrocarbon basins

Tight-gas sandstones are a significant unconventional resource for natural gas. Tight-gas sandstones of the Cretaceous Mesaverde Group in the Piceance basin, Colorado, have been considered continuous, basin-centered gas accumulations (Brown et al., 1986; Johnson, 1989; Law, 2002; Cumella and Scheevel, 2008; Fall et al., 2012, 2015). The system has gas-prone source rocks and low-permeability reservoirs in close proximity to one another and lacks downdip water contacts and the gas accumulation grades vertically across stratigraphic boundaries, forming a continuously saturated gas interval in the deeper parts of the Piceance basin. With continued burial and gas generation, the system became overpressured, leading to subsequent fracturing of the reservoir rocks. Natural fracture formation was thus contemporaneous with gas generation and charge. Fracture opening and subsequent sealing by mineral precipitation provided transient migration pathways and, therefore, dynamic pore-fluid pressure conditions over time (Fall et al., 2012, 2015). Two fractures from core at the SHCT well site, at depths of ~2 and 2.5 km, are partially or completely cemented by quartz cement bridges (Fig. 2d) and euhedral quartz cements that precipitated synkinematically during fracture opening. Quartz cement bridges are defined as isolated cement occurrences that connect across fracture

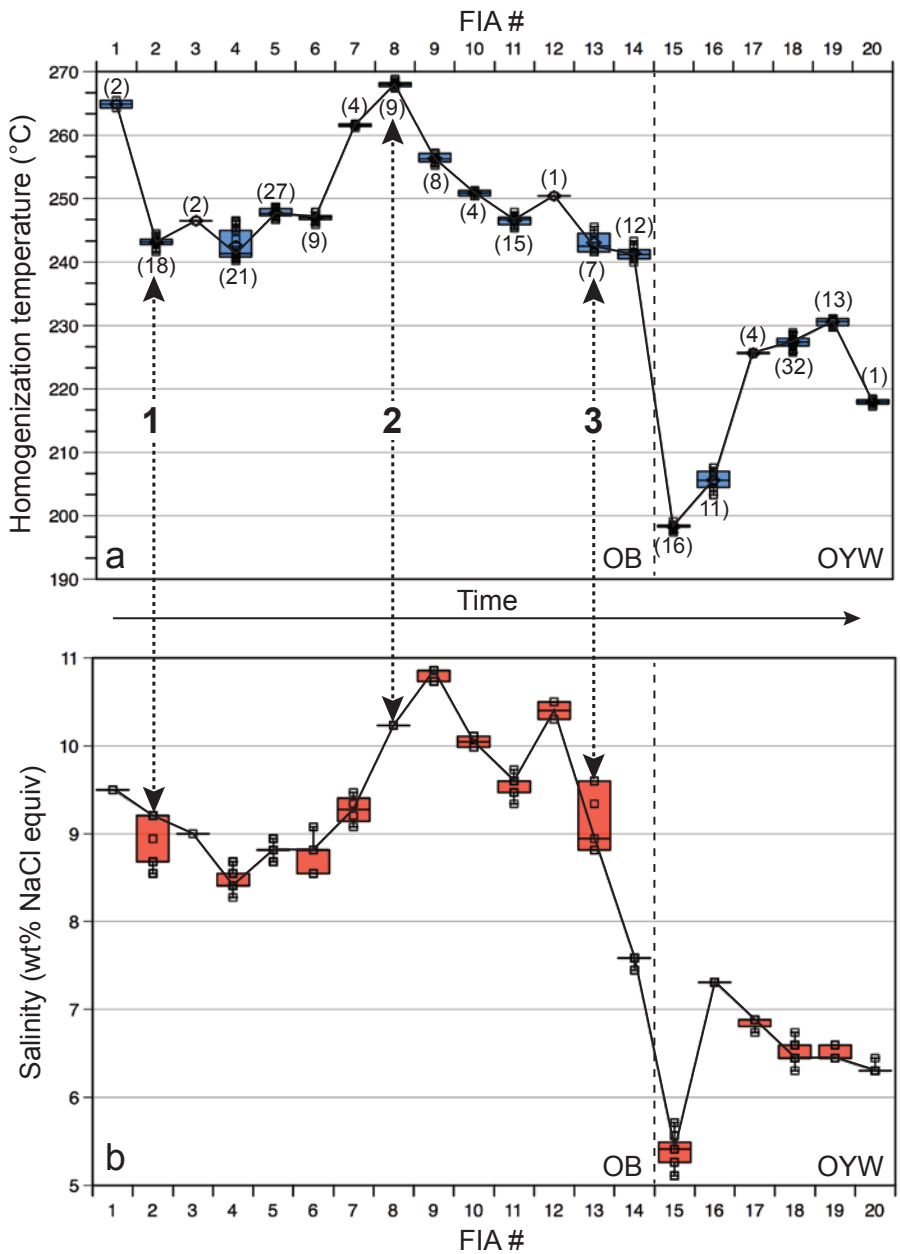

Fig. 4. (a) Homogenization temperatures of fluid inclusions in the color-zoned sphalerite crystal from the OH vein of the Creede epithermal Ag-Pb-Zn deposit, Colorado, shown in Figure 3a, plotted as a function of relative age. (b) Salinities of fluid inclusions in the color-zoned sphalerite crystal from the OH vein of the Creede epithermal Ag-Pb-Zn deposit, Colorado, shown in Figure 3a, plotted as a function of relative age. All data from Roedder, 1974. Plotting fluid inclusion data as a function of relative age and combining homogenization temperature and salinity trends allows one to infer processes associated with formation of the sphalerite crystal. The significant decrease in temperature and salinity between fluid inclusion assemblages (FIAs) 1 and 2 might represent the influx of cooler, lower-salinity meteoric water into the system (arrow 1), whereas the increase in both temperature and salinity from FIAs 6 to 9 could represent a pulse of higher-temperature, more saline magmatic-hydrothermal fluids (arrow 2). Finally, the significant decrease in temperature and salinity following FIAs 13 to 14 could represent collapse of the meteoric water system in the waning stages of magmatic-hydrothermal activity (arrow 3). Abbreviations: OB = orange-brown, OYW = outer yellow-white.

walls and typically grow with the *c* crystallographic axis oriented roughly perpendicular to the fracture walls (Laubach et al., 2004; Lander and Laubach, 2015). High-resolution scanning electron microscopy-cathodoluminescence (SEM-CL) images reveal multiple crack-seal cement layers (Ramsay, 1980; Laubach et al., 2004; Becker et al., 2010) within the core of the bridges. Each crack-seal increment contains an FIA that is oriented parallel to the fracture walls. Textural CL maps of crack-seal cement layers, the lateral cements that deposit on the side of the crack-seal increments, and their mutual crosscutting relationships allowed for interpretation of fracture opening and relative cement sequences. The

Table 2. Minimum and Maximum Range in T_h (ΔT_h) for Individual FIAs from Various Geologic Environments Determined in this Study and Reported in the Literature

No.	Geologic environment	Location	Host mineral	ΔT_h within FIA (°C) Min	Max	Reference
1	Sedimentary basin	Piceance basin, Colorado	Quartz	0.1	5.9	This study; Fall et al., 2012, 2015
2		East Texas basin, Texas	Quartz	0.0	5.0	Becker et al., 2010
3		Green River basin, Wyoming	Quartz	0.5	5.5	Laubach et al., 2016
4		Monterrey, California	Dolomite	2.0	14.0	Eichhubl and Boles, 2000
5	MVT deposits	Cave-in-Rock, Illionis	Fluorite	1.2	9.4	This study
6		Cave-in-Rock, Illionis	Fluorite	0.8	21.5	Richardson and Pinckney, 1984
7		Cave-in-Rock, Illionis	Fluorite	0.6	50.2	Pelch et al., 2015
8		Upton, Quebec, Canada	Barite	0.8	17.8	Paradis et al., 2004
9		Upton, Quebec, Canada	Calcite	2.7	16.3	Paradis et al., 2004
10		Upton, Quebec, Canada	Quartz	5.7	16.7	Paradis et al., 2004
11	Epithermal deposits	Creede, Colorado	Sphalerite	0.1	6.3	Roedder, 1974
12		Waihi, New Zealand	Quartz	2.0	37.0	Brathwaite and Faure, 2002
13		Waihi, New Zealand	Calcite	5.0	47.0	Brathwaite and Faure, 2002
14		Wutong, China	Sphalerite	0.1	20.0	Lecumberri-Sanchez et al., 2014
15		Wutong, China	Quartz	1.0	39.0	Lecumberri-Sanchez et al., 2014
16		Wutong, China	Rhodochrosite	1.0	19.0	Lecumberri-Sanchez et al., 2014
17		Santa Margarita, Mexico	Quartz	0.1	12.2	Moncada and Bodnar, 2012
18		Santa Margarita, Mexico	Calcite	0.4	9.3	Moncada and Bodnar, 2012
19		Santa Margarita, Mexico	Adularia	0.1	4.1	Moncada and Bodnar, 2012
20		La Luz, Mexico	Quartz	0.1	26.0	Moncada et al., 2017
21		La Luz, Mexico	Calcite	0.1	21.0	Moncada et al., 2017
22		La Luz, Mexico	Adularia	2.0	2.0	Moncada et al., 2017
23		Hauraki, New Zealand	Quartz	3.0	49.0	Simpson et al., 2015
24		Patricia, Chile	Quartz	1.0	31.0	Chinchilla et al., 2015
25		Patricia, Chile	Sphalerite	1.0	34.0	Chinchilla et al., 2015
26		Fresnillo, Mexico	Quartz	1.0	59.0	Simmons et al., 1988
27		Fresnillo, Mexico	Sphalerite	2.0	30.0	Simmons et al., 1988
28		Fresnillo, Mexico	Calcite	1.0	30.0	Simmons et al., 1988
29		Hauraki, New Zealand	Quartz	2.0	72.0	Simpson and Mauk, 2011
30		Hauraki, New Zealand	Calcite	4.0	47.0	Simpson and Mauk, 2011
31		Mt. Milligan, Canada	Quartz	1.0	52.0	LeFort et al., 2011
32		Buriticá, Colombia	Quartz	4.0	79.0	Lesage et al., 2013
33		Buriticá, Colombia	Sphalerite	14.0	99.0	Lesage et al., 2013
34		Cerro Negro, Argentina	Quartz	1.0	11.5	Vidal et al., 2016
35		Cerro Negro, Argentina	Adularia	5.9	20.0	Vidal et al., 2016
36		Cerro Negro, Argentina	Calcite	3.0	5.0	Vidal et al., 2016
37		Osilo, Sardinia	Quartz	1.0	53.0	Simeone and Simmons, 1999
38		Rosia Montana, Romania	Quartz	1.0	201.0	Wallier et al., 2006
39		Gandy, Iran	Sphalerite	0.0	30.0	Shamanian et al., 2004
40		Alto de la Blenda, Argentina	Quartz	1.0	19.6	Márquez-Zavalia and Heinrich, 2016
41	Porphyry copper deposits	Bingham, Utah	Quartz	2.3	91.9	This study
42		Copper Creek, Arizona	Quartz	3.5	38.5	This study
43		Altar, Argentina	Quartz	0.0	18.0	Maydagán et al., 2015
44		Morococha, Peru	Quartz	0.0	54.0	Catchpole et al., 2015
45		Nevados de Famatina, Argentina	Quartz	4.0	130.0	Pudack et al., 2009
46		Oyu Tolgoi and Zeseh Uul, Mongolia	Quartz	14.0	102.0	Müller et al., 2010
47		El Teniente, Chile	Quartz	3.0	189.0	Klemm et al., 2007
48		Questa, New mexico	Quartz	2.0	181.0	Klemm et al., 2008
49	Granite-related ore deposit	Mole granite, Australia	Quartz	0.0	145.0	Audétat, 1999; Audétat et al., 2000
50	Pegmatite	Marble Canyon, California	Quartz	2.6	28.3	This study
51	Skarn	Ambohimirahavavy, Madagascar	Quartz	1.0	119.0	Estrade et al., 2015
52	Orogenic gold	Meguma, Nova Scotia, Canada	Quartz	4.1	125.0	This study
53		Chega Tudo, Brazil	Quartz	0.0	270.0	Klein et al., 2008
54		Holy Island, Wales	Quartz	0.5	89.3	Watson, 1999; Stowell et al., 1999
55		Central Alps, Switzerland	Quartz	0.0	14.9	Miron et al., 2013
56		Serra Pelada, Carajás, Brazil	Quartz	21.0	68.0	Berni et al., 2016
57		South Mountain, Nova Scotia, Canada	Quartz	0.0	35.0	Kontak and Kyser, 2011

FIA = fluid inclusion assemblage, MVT = Mississippi Valley-type

formation of the crack-seal texture of the cement bridges is thought to be a consequence of recurring gas charge and fracturing during continuous gas generation within the Piceance basin (Fall et al., 2012, 2015).

Six to 12 FIAs identified in six cement bridges from the two fractures (three from each) trapped two coexisting fluids: two-phase, liquid-rich, methane-saturated aqueous inclusions with salinity from 1 to 2.5 wt % NaCl equiv and single-phase, liquid inclusions containing a methane-dominated hydrocarbon fluid. The two-phase, liquid-rich inclusions contain 5 to 10 vol % vapor and vary in size from <1 to 10 μm. The single-phase inclusions are <1 to 20 μm in size. Homogenization temperatures of the aqueous fluid inclusions vary from ~ 144.2° to 180.5°C, with T_h variation within individual FIAs from 0° to 5.9°C, with the majority showing variations of ~1°C (Fig. 5).

Cave-in-Rock, Illinois: Mississippi Valley-type deposits

Mississippi Valley-type (MVT) deposits are epigenetic hydrothermal lead-zinc ore deposits that are generally hosted by carbonates and occur in sedimentary basins (Leach and Sangster, 1993; Leach et al., 2001, 2005). These deposits form at

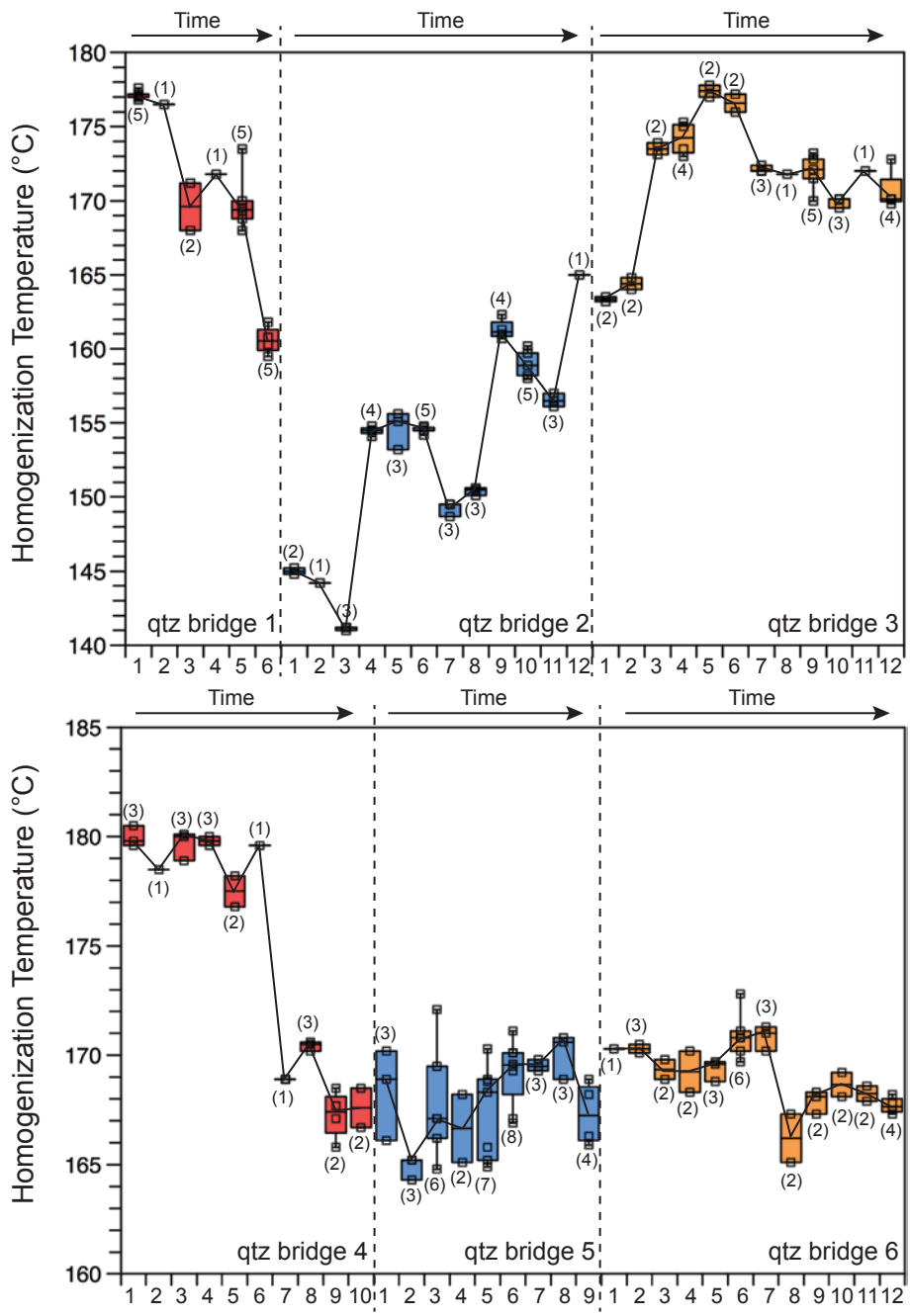

Fig. 5. Measured homogenization temperatures of fluid inclusions within individual fluid inclusion assemblages in quartz (qtz) cement bridges in opening-mode fractures in the Piceance basin, Colorado, plotted according to relative age of the assemblages within each bridge. The data are plotted as described in the text. Data from Fall et al. (2015).

low to moderate temperatures and are associated with highly saline basinal brines. The carbonate-hosted Pb-Zn fluorite-barite deposits of the greater Mississippi Valley in central North America, including the Cave-in-Rock fluorspar district in southern Illinois, represent the best-studied MVT deposits in the world. The Cave-in-Rock fluorspar district is a classic example of the fluorite subtype of the MVT deposits, where fluorite is either the main gangue mineral or is present in economic concentrations. At Cave-in-Rock the fluorite mineralization occurs in veins, breccias, and large bedded replacement deposits (Richardson and Pinckney, 1984; Richardson et al., 1988; Spry et al., 1990; Spry and Fuhrmann, 1994; Kendrick et al., 2002). Fluorite is the main ore mineral; however, smaller amounts of sphalerite, galena, and chalcopyrite also occur. The fluorite crystals are color banded and range from an early yellow variety to late, alternating, purple and white zones. Some individual crystals in large vugs are up to 30 cm on a side.

The fluorites examined here contain two types of primary and one type of secondary inclusions. Irregularly shaped primary inclusions ("primary irregular") (Fig. 1f) occur within thin, color-banded growth zones, usually mixed with solid inclusions. Cubic, tabular, or wedge-shaped (negative crystal-shaped) primary inclusions ("primary cubic") (Fig. 1e) occur within colored growth bands as isolated inclusions or in small clusters. The secondary inclusions occur along healed microfractures (Fig. 2e), usually parallel to the octahedral cleavage directions, and have rounded, oval, elongated, or negative crystal (most of the time gyroid) shapes. The inclusions contain aqueous solutions with >18 wt % NaCl equiv salinity. Some primary and secondary inclusions contain oil (petroleum) or aqueous-oil mixtures and are yellow-brown in appearance and usually contain dark-brown opaque solids that are the result of thermal degradation of the oil (Richardson and Pinckney, 1984). At least some of the primary irregularly shaped inclusions are earlier than some of the primary negative crystal-shaped inclusions, but we cannot prove based on petrography that all of the irregularly shaped primary inclusions are earlier than all of the negative crystal-shaped inclusions. However, all (or at least most) of the secondary inclusions appear to postdate all of the primary inclusions, based on their occurrence on fractures that crosscut all or most of the growth zones. Within each subtype of FIA, i.e., the irregularly shaped primary inclusions, the cubic and negative crystal-shaped primary inclusions, and the secondary inclusions, the relative ages of FIAs could not be determined with confidence.

Microthermometry was carried out on 33 FIAs that could be related to either a growth zone or a healed fracture. Each FIA contained between nine and 56 fluid inclusions (Fig. 6). Ten FIAs consisting of irregularly shaped primary inclusions show average T_h from 152.0° to 156.1°C with T_h variations within an FIA from 5.5° to 9.4°C. Nine small clusters of primary, negative crystal-shaped inclusions yield average T_h from 143.8° to 148.5°C with T_h variation within an FIA from 3.6° to 7.7°C. Average T_h for 14 secondary FIAs trapped along healed microfractures varies from 142.0° to 145.2°C with T_h variations within individual FIAs from 1.2° to 2.8°C (Fig. 6). It is worth noting that the range in T_h for secondary FIAs is generally much smaller than that for primary FIAs; possible explanations for this difference are discussed later.

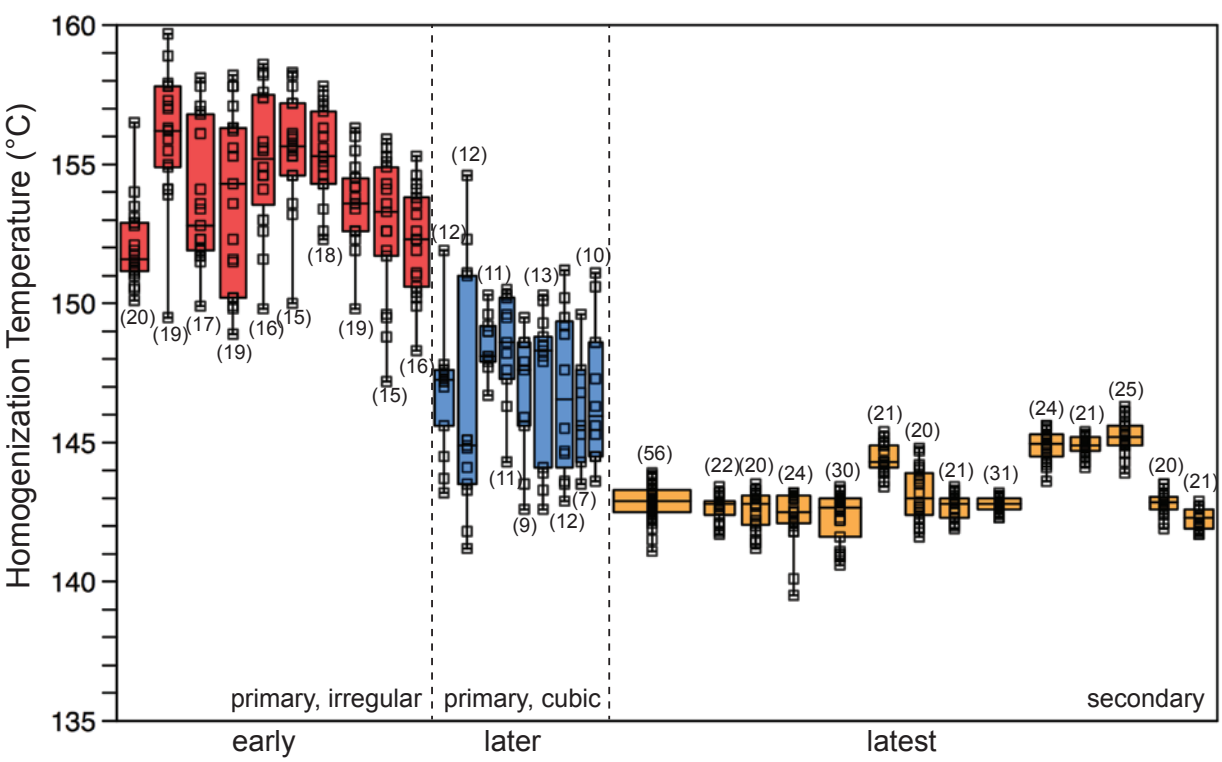

Fig. 6. Measured homogenization temperatures of fluid inclusions within individual fluid inclusion assemblages in fluorite from the Cave-in-Rock fluorspar deposit, southern Illinois, collected as part of this study. Width of boxes for the secondary inclusions proportional to number of inclusions within the fluid inclusion assemblage.

Creede, Colorado: Epithermal deposits

Epithermal deposits develop in shallow volcanic settings as a result of intrusion-related hydrothermal activity (Simmons et al., 2005). Fluid inclusions in epithermal environments typically contain ubiquitous two-phase, liquid-vapor, low-salinity fluids. Vapor-rich inclusions are common in the epithermal environment, and sometimes liquid-rich and vapor-rich fluid inclusions occur in the same FIA, documenting the occurrence of boiling (Bodnar et al., 1985a).

The Creede, Colorado, deposit is a well-known epithermal deposit and was the subject of many studies of the geologic and hydrologic environment (Steven and Eaton, 1975), geochemical aspects (Roedder, 1974; Barton et al., 1977; Bethke and Rye, 1979; Hayba, 1997), and duration and age (Bethke et al., 1976; Campbell and Barton, 2005) of ore deposition. One of the most studied segments of the ore deposit was the OH vein, which is a steeply dipping series of connected tension fractures up to 2 m wide that at depth becomes an open breccia with minor quartz, chlorite, and sulfide mineralization (Barton et al., 1977). The vein was formed through five paragenetic stages, labeled by Bethke and Rye (1979) from A (youngest) to E (oldest). The D stage was the most studied of these, consisting of large, zoned sphalerite crystals that made it possible to develop a sphalerite stratigraphy to correlate crystal growth zones throughout the deposit (Hayba, 1997). The sphalerite crystals are coarse grained (some are 10 cm or more in diameter) and zoned, reflecting variations in iron content, and were subdivided into three substages: inner white-yellow, orange-brown, and outer yellow-white (Fig. 3a). Roedder (1974) studied the fluid inclusions in one such zoned sphalerite crystal, demonstrating changes in temperature and salinity of the ore fluid over time by studying FIAs in 20 different sequential zones.

The T_h data presented here are from Roedder (1974). The analyzed fluid inclusions were mostly primary and pseudosecondary and are mostly large, elongated, and negative crystal shaped. Fluid inclusions from 20 FIAs in sphalerite (each growth zone represents an FIA, as described by Goldstein and Reynolds, 1994, fig. 7.1) show relatively small T_h variation within FIAs (Figs. 3d, 4a). Salinities vary from 5 to 11 wt % NaCl equiv. The 20 FIAs show average T_h from 198.3° to 268.1°C, with T_h variations within individual FIAs from 0° (only two inclusions in the FIA with the same T_h) to 6.3°C.

Bingham Canyon, Utah, and Copper Creek, Arizona: Porphyry copper deposits

Porphyry copper deposits are large, low-grade, epigenetic, intrusion-related copper deposits. Magmatic-hydrothermal fluids play an important role in the formation of porphyry copper deposits. Most of the information on the physical and chemical evolution of these hydrothermal fluids comes from fluid inclusion studies (Roedder, 1971; Moore and Nash, 1974; Reynolds and Beane, 1985; McMillan and Pantaleyev, 1988; Beane and Bodnar, 1995; Bodnar, 1995; Redmond et al., 2004; Landtwing et al., 2005).

A euhedral quartz crystal from an early quartz vein from the Bingham Canyon porphyry copper deposit in Utah that has previously been referred to as quartz type Q1 (Redmond et al., 2004; Landtwing et al., 2005) was examined in this study. A quartz sample from the quartz-cemented granodioritic breccia of the Copper Creek porphyry deposit in Arizona was also examined (Anderson et al., 2009). The hydrothermal quartz veins from these deposits contain a large number of fluid inclusions that precluded the distinction between primary, secondary, or pseudosecondary origin, hence the data were obtained from FIAs trapped along healed microfractures where the contemporaneity of the inclusions was clear. Fluid inclusions from 34 FIAs in quartz from these deposits show relatively large T_h variation within individual FIAs (Fig. 7).

At room temperature, individual FIAs contained one of the following four types of inclusions: liquid-vapor inclusions with a large vapor bubble and opaque phase and intermediate salinity of around 7 to 12 wt % NaCl equiv, inclusions containing brine plus halite and sylvite daughter minerals and sometimes anhydrite daughter crystals, vapor-rich inclusions, and liquid-vapor inclusions with relatively small vapor bubble and salinities of 15 to 20 wt % NaCl equiv. The two-phase inclusions with large vapor bubbles showed evidence for CO_2 during cooling based on the formation of a clathrate phase. Three FIAs consisting of two-phase inclusions with a large vapor bubble are thought to represent fluid trapped in the early stages of the porphyry system evolution (Roedder, 1971; Landtwing et al., 2005) and show average T_h from 360.2° to 378.2°C, with T_h variation within individual FIAs from 10.1° to 11.4°C. Twenty FIAs consisting of brine inclusions that homogenized by vapor disappearance (brine 1) show average T_h from 264° to 563°C, with T_h variations from 2.6° to 62.1°C. Seven FIAs consisting of brine inclusions that homogenize by halite disappearance (brine 2) show average liquid-vapor T_h from 260.4° to 397.7°C, with T_h variations from 9.1° to 75.1°C. Four FIAs, representing the late postore stage at Copper Creek, show average T_h from 339.4° to 346.6°C, with T_h variations from 3.5° to 10.1°C (Fig. 7).

Meguma, Nova Scotia: Orogenic gold deposits

The mesothermal (orogenic) lode gold deposits of the Meguma metamorphic terrane in Nova Scotia, Canada, are Au-rich quartz veins in metaturbiditic rocks of the Meguma Group (Kontak et al., 1990, 2001, 2005, 2011; Kontak and Kerrich, 2002; Kontak and Kyser, 2011). The CO_2-rich, aqueous, ore-forming fluids, characteristic of this environment, are thought to have been generated by metamorphic devolatilization of subcreted hydrated crust (Bierlein and Crowe, 2000).

Fluid inclusions from 27 FIAs in quartz from the Meguma metamorphic lode-gold deposit were studied (Fig. 8). No petrographic evidence that could be used to identify primary inclusions was observed, and three different types of secondary inclusions, based on chemical composition and room temperature phase relations, are present. One type contains H_2O-CO_2 with 10 to 15 mol % CO_2. A second type contains low-salinity H_2O-NaCl (<1–2 wt % NaCl equiv) liquid plus a vapor bubble. The third, less common, type of inclusion contains halite daughter minerals in addition to liquid and vapor. This latter type showed extremely heterogeneous phase ratios within the same FIA, and petrographic evidence of necking is observed. For this reason, T_h data were not collected from these halite-bearing FIAs. All three types of fluid inclusions occur along healed microfractures; however, textural properties of the host observed under crossed polars (different

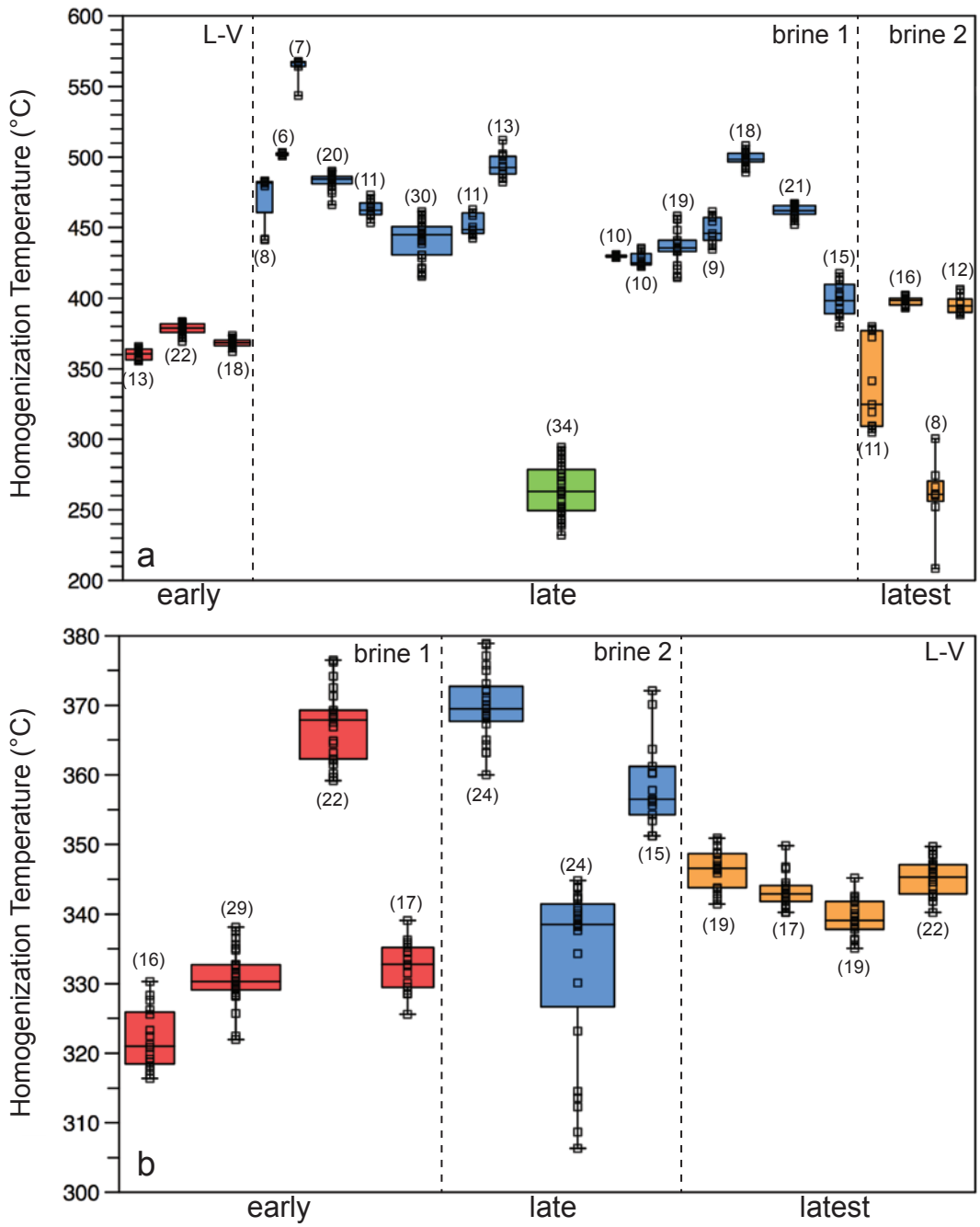

Fig. 7. Homogenization temperature variations within individual fluid inclusion assemblages in quartz from the Bingham Canyon, Utah, porphyry copper deposit (a) and the Copper Creek, Arizona, porphyry copper deposit (b) obtained in this study. Brine 1 = halite-bearing inclusions that homogenize by vapor disappearance, brine 2 = halite-bearing inclusions that homogenize by halite disappearance, L-V = liquid-vapor.

extinction angles of the quartz along healed microfractures) suggest that the low-salinity H_2O-NaCl inclusions are later than the carbonic inclusions. This paragenesis is consistent with the observations of Robert et al. (1995) for similar lode-gold quartz veins in the Val d'Or district of the southeastern Abitibi greenstone belt, Canada. The 14 H_2O-NaCl FIAs show average T_h from 207.9° to 307.8°C, with T_h variations within individual FIAs from 5.7° to 125°C. The 13 H_2O-CO_2 FIAs show average T_h from 272.5° to 308.6°C, with T_h variations from 3.6° to 24.9°C (Fig. 8). One FIA in the Meguma sample showed a 125°C range in T_h (163.3°–289°C), and this FIA is discussed in more detail below.

Marble Canyon granitic pegmatite

Pegmatites form from residual melts generated during crystallization of granitic magmas and are enriched in incompatible components, fluxing agents, volatiles, and rare earth elements (Černý, 1991; Černý and Ercit, 2005; Simmons and Webber,

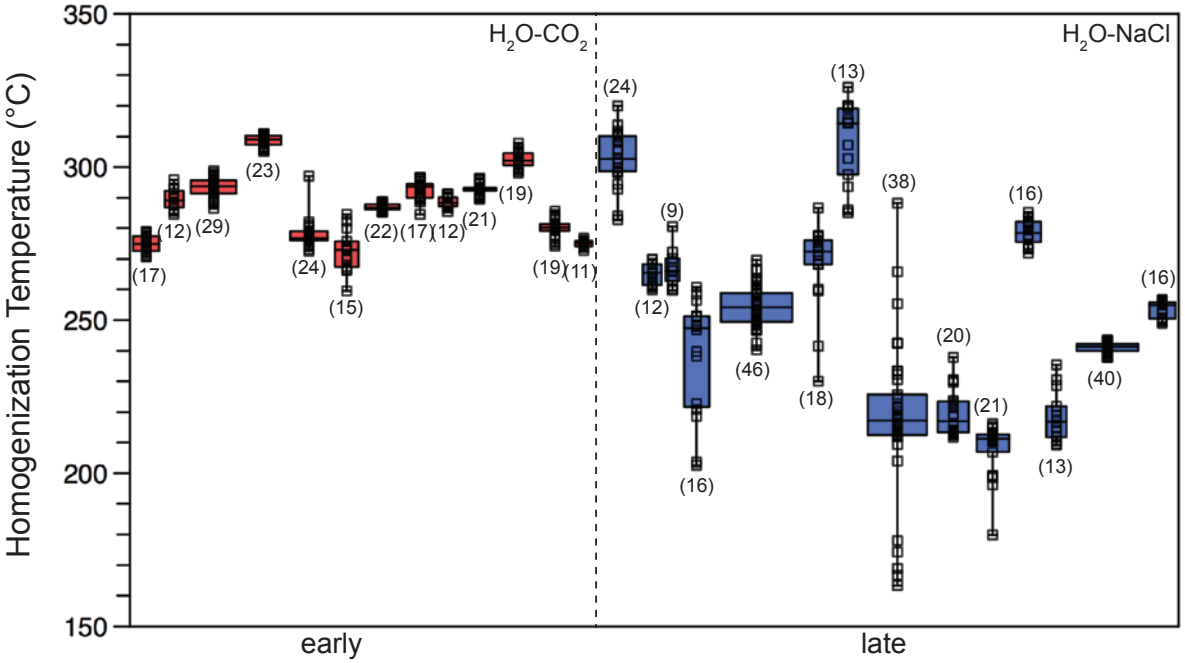

Fig. 8. Measured homogenization temperatures of fluid inclusions within individual fluid inclusion assemblages in quartz from the orogenic lode gold deposits of the Meguma metamorphic terrane, Nova Scotia, Canada, obtained in this study.

2008). Primary and pseudosecondary FIAs are observed in pegmatitic minerals, but the relationship between the fluid inclusions and pegmatite formation is uncertain.

The Marble Canyon pegmatite is an intrusion in the contact aureole of the composite Eureka Valley-Joshua Flat-Beer Creek pluton in the Deep Springs Valley-Eureka Valley region of the White-Inyo Mountains of eastern California (J. Student, pers. commun., 2006). The Jurassic Eureka Valley-Joshua Flat-Beer Creek pluton is characterized by three principal units: the Eureka Valley monzonite, the Joshua Flat quartz monzonite, and the Beer Creek granite (Coleman et al., 2005; Straathof et al., 2006; Jackson et al., 2007; Reynolds et al., 2007). The recently discovered pegmatitic body contains large crystals of feldspars, quartz, and micas and minor schorl. Also, small pockets with quartz, axinite, and associated fluorite were observed. Much of the axinite is massive and occurs in fractures associated with pneumatolytic fracturing of the pegmatite. The pegmatite is on strike with the aplite dikes of the Eureka Valley-Joshua Flat-Beer Creek pluton, which have been boudinaged in the aureole. This relationship suggests that the pegmatite is associated with the Eureka Valley-Joshua Flat-Beer Creek magmatism (J. Student, pers. commun., 2006).

The large quartz crystals found in pockets in the Marble Canyon pegmatite are zoned with a smoky quartz core and a clear outer rim, separated by a thin, dark growth zone. The quartz crystals contain well-defined FIAs of primary, pseudosecondary, and secondary inclusions. The core contains secondary, two-phase liquid + vapor inclusions, and pseudosecondary halite-bearing inclusions along trails that start in the dark growth zone and extend into the core. The dark growth zone contains primary halite-bearing inclusions, similar to the pseudosecondary inclusions that occur in the core. The outer clear rim contains secondary halite-bearing inclusions that represent a later generation of high-salinity fluids.

The fluid inclusions in this sample contain a solution approximated by the system H_2O-NaCl-$CaCl_2$, confirmed by low initial ice-melting temperatures (~–52°C), with varying amounts of $CaCl_2$ and NaCl. The secondary inclusions restricted to the core have a salinity below halite saturation and a high $CaCl_2$ concentration that was confirmed by formation of antarcticite ($CaCl_2 \cdot 6H_2O$) during cooling that was identified using Raman spectroscopy. The primary inclusions trapped along the growth zone and the pseudosecondary trails that start in the growth zone and extend into the core contain halite-saturated solutions, with a salinity (determined from the halite dissolution temperature) of around 30 wt % NaCl equiv (Bodnar and Vityk, 1994). The outer clear zones of the crystals contain secondary, halite-bearing inclusions with a salinity of about 33 wt % NaCl equiv, and antarcticite was not observed during cooling. This succession suggests the presence of Ca-rich salt solutions early in the crystallization history that evolved toward a more Na-rich and Ca-poor composition with time. The high salinity of the magmatic fluids in the Marble Canyon pegmatite is consistent with chlorine partitioning data that suggest that in deeper magmatic systems the early fluids should have high salinities (Cline and Bodnar, 1994). Four secondary FIAs in the core show average T_h from 255.6° to 276.6°C, with T_h variations within individual FIAs from 2.9° to 14.6°C. Two primary and three pseudosecondary FIAs show average T_h from 234.4° to 254.5°C, with T_h variations from 5.3° to 28.3°C. The secondary inclusions in the clear rim have average T_h from 253.8° to 284.5°C, with T_h variations from 2.6° to 15.3°C (Fig. 9).

Summary of Ranges in Homogenization Temperatures in Different Geologic Environments

Ranges in fluid inclusion T_h within individual FIAs measured in this study were combined with data from the literature to

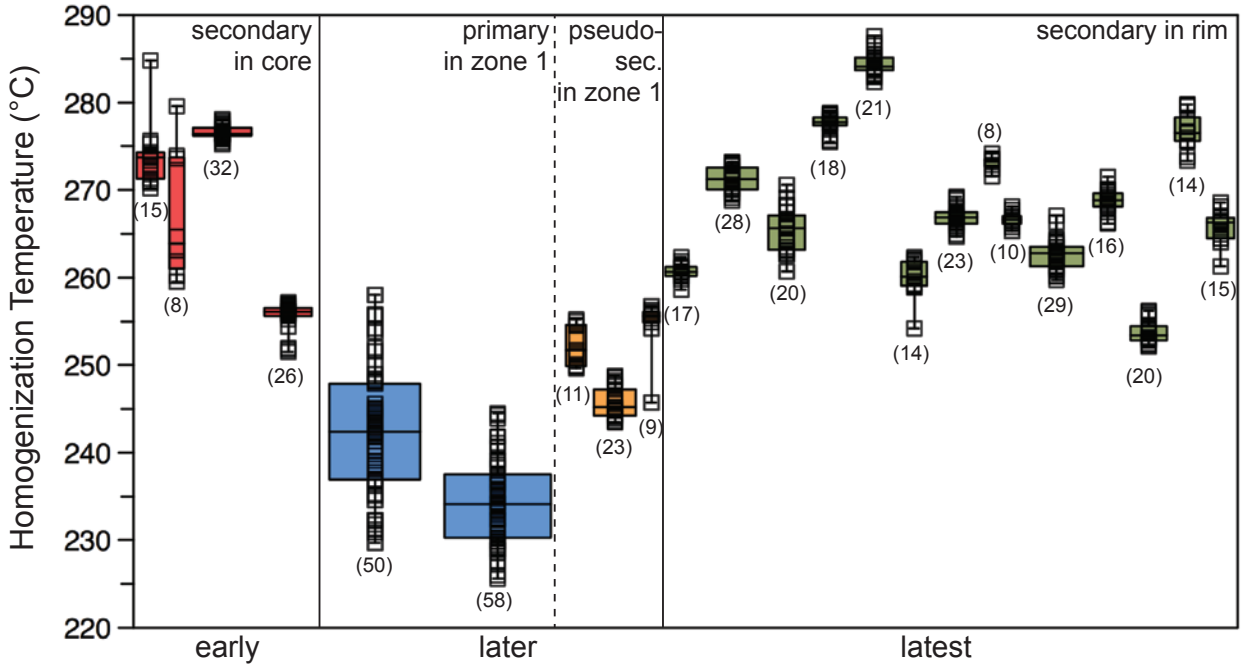

Fig. 9. Measured homogenization temperatures of fluid inclusions within individual fluid inclusion assemblages from the Marble Canyon pegmatite, California, obtained in this study.

develop a more comprehensive assessment of ranges in T_h that are achievable in different environments. The first criterion used to filter the data was whether the authors of published data stated explicitly that they followed the FIA protocol in collecting data. Many authors stated that they did follow the FIA protocol, but upon examination of the data it was clear that they did not, for various reasons. These studies and data were excluded from further consideration. Finally, if the authors stated that they followed the FIA protocol, and if the text and data in the paper supported this statement, and if the workers provided the microthermometric data for all of the fluid inclusions in all of the FIAs, then those data were used in this study. If the published data met these criteria, we did not further filter the results; for this reason, some FIAs from the literature show a wide range in T_h. Results for different environments examined in this study are summarized below. Note that T_h ranges in FIAs for the observed environments that are plotted on the figure below are plotted on a log scale. Additionally, when the range in T_h equals 0.0°C, the data are plotted on the 0.1°C line because a 0.0°C range cannot be plotted on a log scale.

Tight-gas (low-permeability) sandstone environments

Data from the Piceance basin from this study were combined with previously published data from other similar environments to assess the range in T_h within an FIA that is achievable in such an environment (Fig. 10; Table 2). Figure 10 shows the total range in measured T_h for 144 FIAs in quartz bridges from this environment. Analysis of the data shows that five out of 144 FIAs show identical T_h for all fluid inclusions in the assemblage (range = 0°C), and 49 out of 144 FIAs show a range of 1°C or less. The median range in T_h for all 144 FIAs considered is 2°C, with a range from 2.7°C (first quartile, Q1) to 3.7°C (third quartile, Q3). The results indicate that the temperature of the majority of fluid events in tight-gas reservoirs represented by FIAs can be constrained to better than 2°C (the median range).

MVT deposits

Combining data from the Cave-in-Rock fluorite deposit collected in this study with microthermometric data from other MVT deposits allows us to assess the range in T_h that one

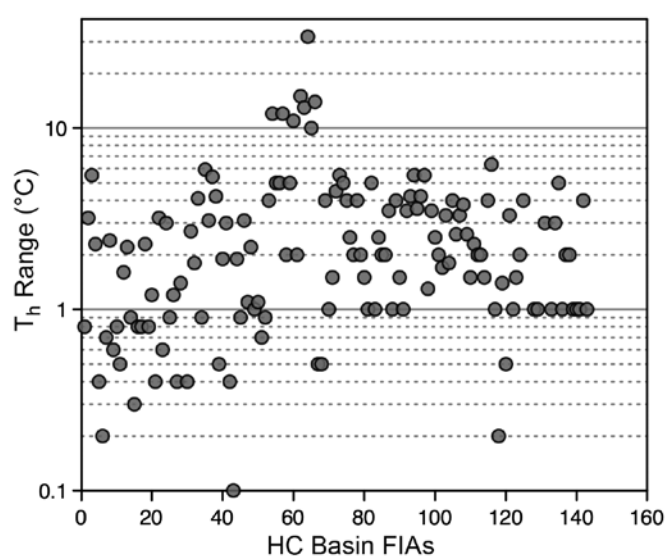

Fig. 10. Total range in homogenization temperature (T_h) within individual fluid inclusion assemblages (FIAs) shown on a log scale from low-temperature, low-permeability, sedimentary environments (HC basins). The data are from this study and the literature and are listed in Table 2. Each data point represents the total range in temperature observed within each of the 144 individual FIAs rom HC basins reported in this study, with the FIA number plotted on the x-axis corresponding to the FIA number listed in Electronic Appendix Table A1.

might expect for a given FIA in this environment, and data are compiled in Figure 11 and Table 2. Analysis of the data shows one FIA with identical T_h for all fluid inclusions in the assemblage (range = 0°C), and 11 out of 116 FIAs show a range of 1°C or less. The median range in T_h for all 116 FIAs considered is 4.1°C, with a range from 2.3°C (Q1) to 8.3°C (Q3). The results show that it should be possible to constrain the temperature of a thermal event in the MVT environment to better than ~4°C. We note that most of the literature data for MVT deposits that was incorporated into this study is for fluid inclusions in calcite, and we propose that the results reported here are applicable to fluid inclusions in both fluorite and calcite from the MVT environment.

Epithermal deposits

Data from the Creede epithermal deposit were combined with previously published data from other epithermal deposits to assess the achievable range in T_h for an individual FIA (Fig. 12; Table 2). Figure 12 shows data for 923 FIAs from epithermal systems. Analysis of the data shows that 24 out of 923 FIAs show identical T_h for all fluid inclusions in the assemblage (range = 0°C), and 102 out of 923 FIAs show a range of 1°C or less. The median range in T_h for all 923 FIAs considered is 9°C, with a range from 3.8°C (Q1) to 19°C (Q3). While a significant number of FIAs from the epithermal environment show ranges in T_h that extend to several tens of degrees or more, many FIAs show very narrow ranges in T_h. Our results suggest that the temperature of the majority of fluid events in the epithermal environment, as represented by FIAs, can be constrained to better than 9°C (the median range).

Porphyry copper deposits

Data from the Bingham Canyon and Copper Creek porphyry systems from this study were combined with previously published data to gain a broader perspective of the achievable range in T_h within individual FIAs from the porphyry copper environment (Fig. 13; Table 2). While the total range in T_h for porphyry copper systems is similar to that observed for epithermal deposits, a larger proportion of FIAs show a range of >10°C (Fig. 13). Analysis of the data for porphyry deposits shows that 11 out of 271 FIAs show identical T_h for all fluid inclusions in the assemblage (range = 0°C), and 24 out of 271

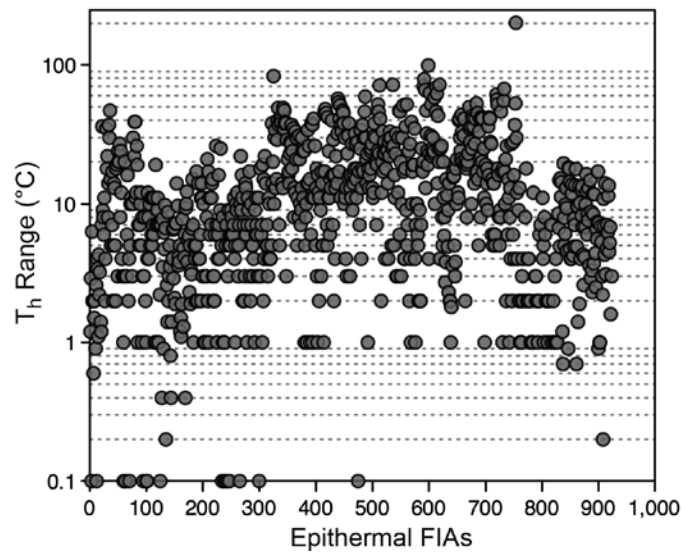

Fig. 12. Total range in homogenization temperature (T_h) within individual fluid inclusion assemblages (FIAs) shown on a log scale from various epithermal precious and base metal deposits reported in the literature; the data are listed in Table 2. Each data point represents the total range in temperature observed within each of the 923 individual FIAs from epithermal deposits reported in this study, with the FIA number plotted on the x-axis corresponding to the FIA number listed in Electronic Appendix Table A1.

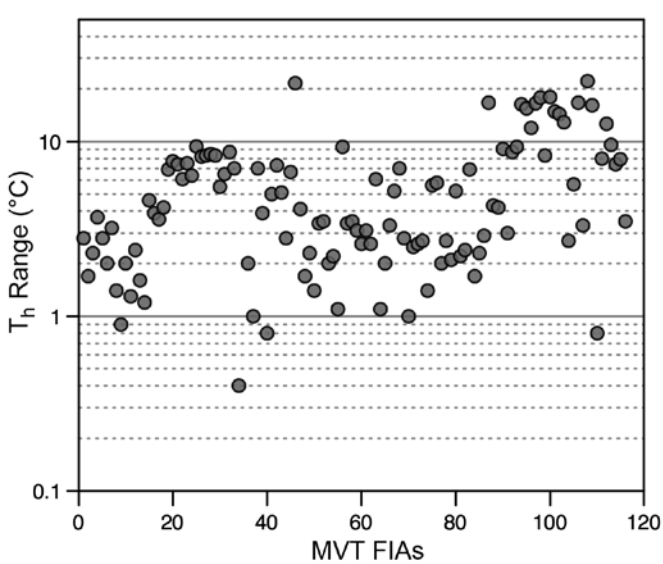

Fig. 11. Total range in homogenization temperature (T_h) within individual fluid inclusion assemblages (FIAs) shown on a log scale from various Mississippi Valley-type (MVT) deposits obtained in this study and reported in the literature, as shown in Table 2. Each data point represents the total range in temperature observed within each of the 137 individual FIAs from MVT deposits reported in this study, with the FIA number plotted on the x-axis corresponding to the FIA number listed in Electronic Appendix Table A1.

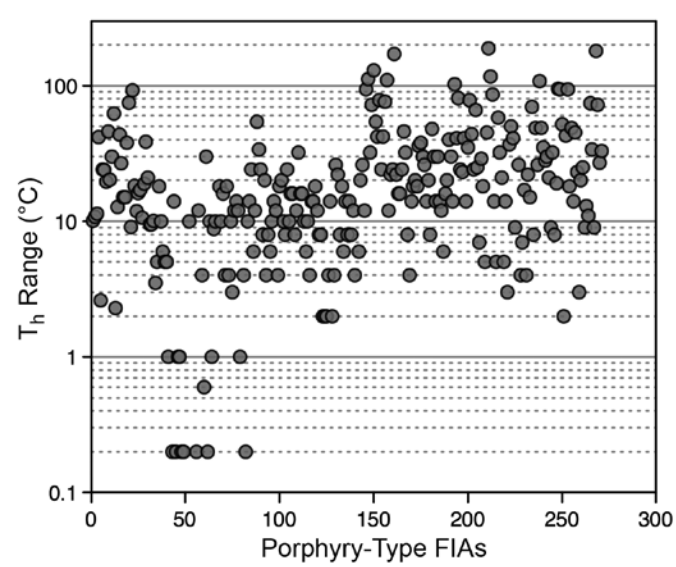

Fig. 13. Total range in homogenization temperature (T_h) within individual fluid inclusion assemblages (FIAs) shown on a log scale from porphyry-type deposits obtained in this study and reported in the literature; the data are listed in Table 2. Each data point represents the total range in temperature observed within each of the 271 individual FIAs from porphyry deposits reported in this study, with the FIA number plotted on the x-axis corresponding to the FIA number listed in Electronic Appendix Table A1.

FIAs show a range of 1°C or less. The median range in T_h for all 271 FIAs considered is 15°C, with a range from 8°C (Q1) to 30°C (Q3). While a significant number of FIAs from the porphyry environment show ranges in T_h that extend to several tens of degrees or more, many FIAs show relatively narrow ranges in T_h. These results suggest that the temperature of the majority of fluid events in the porphyry environment, as represented by FIAs, can be constrained to better than 15°C (the median range). We also suggest that these ranges should be generally applicable to all magmatic-hydrothermal environments associated with shallow intermediate composition magmas, but more study is required to confirm this.

Orogenic gold deposits

Data from the Meguma orogenic gold deposit collected in this study were combined with previously published data reported for well-characterized FIAs in orogenic gold deposits to assess the ranges in T_h for individual FIAs. As shown in Figure 14 and Table 2, the range in T_h for FIAs from orogenic gold deposits is generally greater than that observed in most other deposits, and likely reflects the fact that fluid inclusions from metamorphic environments are more likely to reequilibrate after trapping, as discussed in more detail below.

Analysis of the data for orogenic gold deposits shows that nine out of 231 FIAs show identical T_h for all fluid inclusions in the assemblage (range = 0°C), and 21 out of 231 FIAs show a range of 1°C or less. The median range in T_h for all 231 FIAs considered is 8.7°C, with a range from 4°C (Q1) to 20°C (Q3). While a significant number of FIAs from the orogenic gold environment show ranges in T_h that extend to several tens of degrees or more, many FIAs show relatively narrow ranges in T_h. Our results suggest that the temperature of the majority of fluid events in the orogenic gold environment, as represented by FIAs, can be constrained to better than ~9°C (the median range).

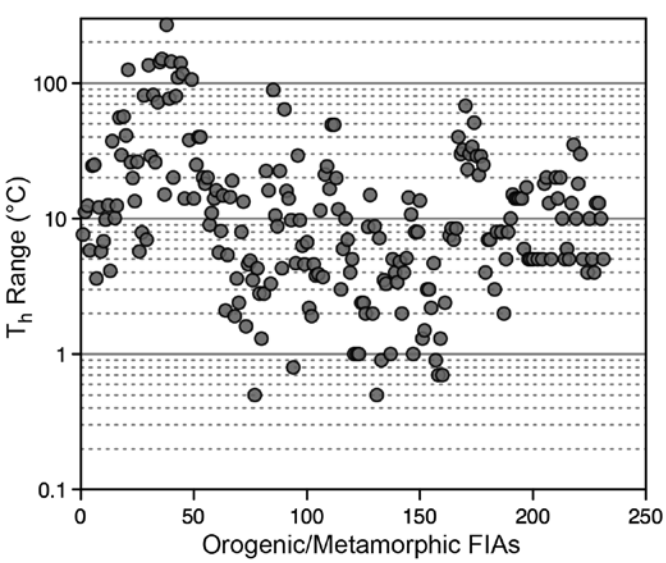

Fig. 14. Total range in homogenization temperature (T_h) within individual fluid inclusion assemblages (FIAs) shown on a log scale from orogenic and intrusion-related gold deposits and other metamorphic environments obtained in this study and reported in the literature; data are listed in Table 2. Each data point represents the total range in temperature observed within each of the 231 individual FIAs from orogenic gold deposits reported in this study, with the FIA number plotted on the x-axis corresponding to the FIA number listed in Electronic Appendix Table A1.

Pegmatites

A search of the literature failed to identify fluid inclusion data from pegmatites that were collected within the FIA framework. Therefore, it was not possible to supplement our limited results with data from the literature to better constrain the range in T_h that might be achievable or expected in pegmatite systems.

Skarns

We did not obtain data for skarn deposits in this study; however, one published study (Estrade et al., 2015) reported data for 52 FIAs from a rare metal skarn. The data show T_h for individual FIAs that range from 1° to 119°C, with a median range of 22.5°C. We note that the FIAs studied were in quartz that represents a later, postore stage in the skarn evolution.

Many studies of skarn deposits include data from fluid inclusions, but data for individual FIAs are usually not reported. This reflects the fact that minerals formed in the early, anhydrous prograde skarn stage, including pyroxene and garnet, often contain only one or a few inclusions in each mineral grain, and the crystals lack internal zoning that can be used to correlate inclusions from one crystal to another. As an example, Meinert et al. (1997) report that pyroxene from the Big Gossan Cu-Au skarn deposit in the Ertsberg district, Irian Jaya, homogenizes over the range from 320° to 485°C. Each individual mineral grain contains only one or a few fluid inclusions, thus precluding application of the more conventional approach to identify FIAs. Alternatively, it is reasonable to assume that the fluid inclusions in pyroxene in toto represent an FIA that was formed early in the paragenesis during the prograde stage of skarn formation. While this interpretation is consistent with the definition of an FIA, it requires that the inclusions within the FIA were trapped over a considerable range in temperature and/or pressure to explain the observed range in T_h. Application of modern imaging and mineral characterization techniques such as cathodoluminescence, Raman mapping, trace element zonation, and others may provide insights into the complex formation history of early skarn phases and allow fluid inclusions to be placed into more restricted groupings.

Intrusion-related gold deposits

As with the skarn deposits, we did not collect data from intrusion-related gold deposits but found literature data for 53 FIAs from a single deposit (Kontak and Kyser, 2011). Reported ranges in T_h for individual FIAs vary from 0° to 35°C, with a median range of 7°C, with a range from 5°C (Q1) to 14°C (Q3). More data from intrusion-related gold deposits systems are needed to better constrain the uncertainty associated with temperatures of fluid events in these systems.

Discussion

Potential causes for T_h variation within FIAs

Ideally, we should expect that if all the fluid inclusions within an FIA are trapped at the same time and at the same temperature and pressure, all the inclusions within the FIA should

homogenize at the same temperature. The results show that it is rare for all the inclusions within the FIA to homogenize at the same temperature, and the observed range in T_h within an FIA is significantly larger than the analytical precision (±0.05°C) with which T_h can be measured. Here, we consider some of the factors that could produce variability in the T_h within a given FIA.

Synthetic fluid inclusions—the ideal case: While it is generally assumed that all fluid inclusions within an FIA were trapped at the same temperature and pressure, it is not possible to know if this is actually the case for natural fluid inclusions. However, synthetic fluid inclusions can be trapped at essentially constant pressure-temperature conditions and, therefore, represent a reasonable reference point from which to begin to examine natural inclusions. Over the past several decades, numerous synthetic fluid inclusion studies have been conducted, and often the data for individual fluid inclusions are reported in publications describing the results. Figure 15 shows measured liquid-vapor T_h ranges of synthetic fluid inclusions trapped under a variety of conditions. Homogenization temperatures of low-salinity aqueous salt inclusions trapped in the one-phase liquid field show low dispersion with median ranges in T_h of 1.5° and 3.4°C, respectively, for pure H_2O (Fig. 15, fluid inclusion type 1) and H_2O-KCl inclusions (Fig. 15, fluid inclusion type 2). Homogenization temperatures of low-salinity aqueous salt inclusions trapped in the one-phase at pressure-temperature conditions near the critical isochore (Fig. 15, fluid inclusion types 3 and 4) also show low median ranges in T_h but show much more variability. Natural halite-bearing fluid inclusions, such as those that occur in the porphyry copper environment, show homogenization either by disappearance of the vapor bubble (Fig. 15, fluid inclusion type 5) or by halite dissolution (Fig. 15, fluid inclusion type 6). While both types show similar median ranges in liquid-vapor T_h, assemblages that homogenize by vapor-bubble disappearance show much less variability than liquid-vapor T_h of inclusions that homogenize by halite disappearance. Fluid inclusions that contain a gas phase, either methane (Fig. 15, fluid inclusion type 7) or carbon dioxide (Fig. 15, fluid inclusion types 8–13), generally show higher median ranges in T_h

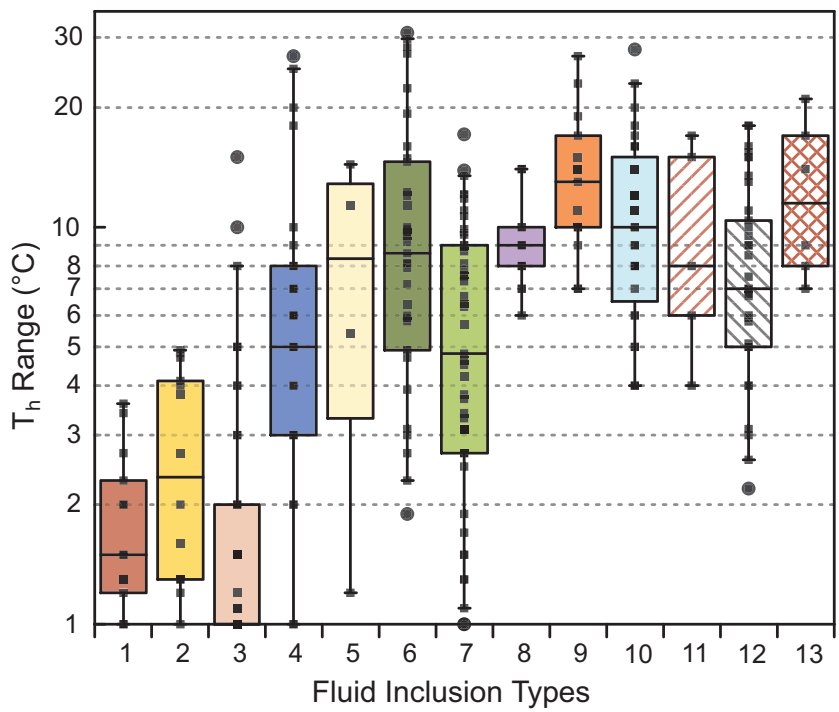

Fig. 15. Measured ranges in liquid-vapor homogenization temperatures (T_h) of synthetic fluid inclusions (SFIs) shown on a log scale trapped at essentially constant temperature and pressure. The different fluid inclusion types shown include the following: (1) pure H_2O SFIs trapped in the one-phase field; all homogenize to liquid (Bodnar and Sterner, 1985); (2) H_2O-20 wt % KCl trapped in the one-phase field; all homogenize to liquid (Bodnar and Sterner, 1985); (3) H_2O-$FeCl_2$; all were trapped in the one-phase field (Steele-MacInnis et al., 2015); (4) H_2O-$CaCl_2$; some were trapped in the one-phase field and some in the two-phase field (Oakes et al., 1994); (5) halite-bearing SFIs trapped in the two-phase (liquid + vapor) field (Bodnar et al., 1985b); (6) halite-bearing SFIs that homogenize by halite-disappearance; the liquid-vapor homogenization temperatures are plotted (Bodnar, 1994); (7) H_2O-CH_4; all fluid inclusions were trapped in the one-phase field, and all homogenize to the liquid phase (Lin and Bodnar, 2010); (8) H_2O-NaCl-CO_2 fluid inclusions containing 6 wt % NaCl equiv and 10 mol % CO_2; all fluid inclusions were trapped in the one-phase field (Schmidt and Bodnar, 2000); (9) H_2O-NaCl-CO_2 fluid inclusion containing 6 wt % NaCl equiv and 20 mol % CO_2; all fluid inclusions were trapped in the one-phase field (Schmidt and Bodnar, 2000); (10) H_2O-NaCl-CO_2 fluid inclusion containing 20 wt % NaCl equiv and 10 mol % CO_2; all fluid inclusions were trapped in the one-phase field (Schmidt and Bodnar, 2000); (11) H_2O-NaCl-CO_2 fluid inclusion containing 20 wt % NaCl equiv and 20 mol % CO_2; all fluid inclusions were trapped in the one-phase field (Schmidt and Bodnar, 2000); (12) H_2O-NaCl-CO_2 fluid inclusions containing 40 wt % NaCl equiv and 5 mol % CO_2; all fluid inclusions were trapped in the one-phase field (Schmidt et al., 1995; Schmidt and Bodnar, 2000); (13) H_2O-NaCl-CO_2 fluid inclusions containing 40 wt % NaCl equiv and 10 mol % CO_2; all fluid inclusions were trapped in the one-phase field (Schmidt and Bodnar, 2000).

and more variability in the range in T_h compared to non-gas-bearing compositions. The observed behavior of synthetic H_2O-CO_2-salt inclusions is consistent with observations in natural environments.

In summary, synthetic fluid inclusions that were trapped under nearly ideal conditions of constant temperature and pressure and that were quenched along an isochore to avoid over- or underpressurizing the fluid inclusion show variations in T_h within a given sample that range from a few to >10°C. Moreover, low-salinity inclusions trapped in the one-phase liquid field show less variability compared to both higher-salinity and gas-bearing compositions. All these observations are consistent with results from natural FIAs. While variations of 1° to 3°C in T_h of fluid inclusions that were all trapped at essentially the same pressure-temperature conditions could reflect the effect of fluid inclusion volume on T_h (Fall et al., 2009; see details below), the causes for the larger variations are unknown, and a discussion of possible causes is beyond the scope of this investigation.

Variations associated with trapping and post-trapping history in nature: One possible cause of variations in T_h within an individual FIA is temperature and/or pressure variations during trapping. If the temperature and/or pressure varies while fluid inclusions are being trapped to produce the FIA, a range in T_h will result, with the magnitude of the range a function of the PTX formation conditions and their variation during inclusion trapping. Goldstein and Reynolds (1994) describe examples in which FIAs are trapped in relatively thick growth zones that form as the temperature of the system changes. If petrographic evidence to determine which inclusions may be early or late is absent, all the inclusions would be grouped into the same FIA and the inclusions would (likely) show some measurable range in T_h.

The relative change in temperature (and pressure) during formation of an FIA is indirectly related to the amount of time required for all the inclusions in an FIA to form. The amount of time required to form a growth zone or heal a microfracture depends, among other factors, on the solubility of the host mineral, and this is related to the temperature, pressure, and fluid chemistry in the specific environment (Rimstidt, 1997). Browne et al. (1989) studied growth rates of minerals in the Ngatamariki geothermal field, New Zealand, and found that prehnite crystals in geothermal wells grew at a rate of 0.2 to 0.5 μm per day perpendicular to the growth surface. At this rate, a 100-μm-thick growth zone could form in 200 to 500 days. Growth rates in the wells may have been accelerated by loss of CO_2 from the upwelling geothermal waters.

Smith and Evans (1984) conducted an experimental study and showed that fractures in single quartz crystals healed/sealed in hours to two days in the presence of pore fluid at 200 MPa pressure at 200°, 400°, and 600°C temperatures. They observed that the extent of healing depends on the temperature (almost complete healing at temperatures ≥400°C), initial silica concentration of the pore fluids, and the initial fracture dimensions. Similar experimental and theoretical studies (Brantley et al., 1990; Brantley, 1992) related to crack healing/sealing in quartz at hydrothermal conditions showed that microfractures 100 μm long and 10 μm wide heal in about 4 h at 600°C and 200 MPa in the presence of pure water, and at 200°C the fractures heal/seal in about 40 days to 1,000 years. In a similar study, Teinturier and Pironon (2003) showed that microfractures in fluorite healed/sealed in 82 to 257 h in the presence of an NH_4Cl-H_2O solution at 200°C and saturation pressure. They also showed that microfractures in quartz healed/sealed in about three days in the presence of NaCl-H_2O solution at 400 bar as the temperature of the system decreased from 400° to 300°C, while a quartz overgrowth band of about 20 μm formed in about two days. All these studies show that growth zones can form, and fractures can heal/seal in a short period of time.

In tight-gas sandstone reservoirs it is estimated that the fracturing event lasts millions of years (up to 35 m.y. in the Piceance basin [Fall et al., 2012, 2015] and up to 48 m.y. in East Texas basin [Becker et al., 2010; Fall et al., 2016]). Fracturing in these basins was driven by periodic pore-fluid overpressures in the reservoir sandstones owing to continuous gas generation and charge. Becker et al. (2010) showed that fractures in the East Texas basin opened over ~42 to 48 m.y. at a rate of ~16 to 23 μm/m.y., while the width of individual crack-seal cements varied from 2 to 15 μm (Becker et al., 2010; Alzayer et al., 2015). This implies that the amount of time required for fracture cement precipitation and inclusion trapping was less than that suggested by the fracture opening rate, and this is consistent with the very narrow range in T_h observed in this environment.

Garven and Raffensperger (1997) describe a numerical fluid flow model for the formation of ore deposits in sedimentary basins, including the MVT deposits. Their time-temperature evolution for a location on the flanks of the Nashville dome, near the location of the southern Illinois fluorspar district, predicts a transient thermal high of 148°C after 70,000 years of fluid flow, and the temperature at this location decreases linearly to 115°C after 700,000 years of flow. This corresponds to an average temperature decrease (148 – 115 ÷ 700,000 – 70,000) of 5.2×10^{-5}°C/yr. The primary negative crystal-shaped inclusions at Cave-in-Rock show minimum T_h variations of 3° to 4°C, with the majority varying from 4° to 7°C (Fig. 6). At a cooling rate of 5.2×10^{-5}°C/yr, between 50,000 and 135,000 years would be required to produce temperature changes of 3° to 7°C. The time to produce the temperature ranges observed in the irregularly shaped primary inclusions would be even longer—up to 150,000 years. The secondary inclusion temperature variations could occur in ≈20,000 years. However, Teinturier and Pironon (2003) have shown that microfractures in fluorite can heal in as little as 82 h at 200°C. Thus, it appears that temperature variation alone cannot account for the observed variation in T_h for MVT deposits, even for those FIAs that show the smallest T_h variation.

Epithermal deposits form in the shallow volcanic environment above a cooling pluton. The formation of the OH vein at Creede, Colorado, was controlled by an overlying aquitard. The low-permeability zone forced the upwelling hydrothermal fluids to flow laterally along the vein (Hayba, 1997), consistent with zoning of the sphalerite crystals along the length of the vein. The abrupt color changes between the growth zones of the crystals suggest that the nature of the ore fluid changed abruptly. Within each growth zone, however, the nature of the fluid was approximately constant along the entire vein (Roedder, 1974; Hayba, 1997), as demonstrated

by the similar compositions of the fluid inclusions within the same FIA.

Fluid inclusion assemblages within the studied sphalerite from the Creede epithermal deposit show T_h variations as low as 1°C, with a majority between 1° and 3°C (Fig. 5a). Barton et al. (1977) developed a combined thermodynamic-geochemical-hydrologic model for the Creede system and reported that at a flow rate of 0.5 cm/s it would take about 500 days for a given volume of fluid to circulate through the orebody. During this time, about 500 μm of sphalerite would precipitate. A sphalerite crystal with an overall thickness of about 8 cm would have been deposited in about 200 years. If we assume that the sphalerite crystal shown in Figure 3a formed in 200 years as the temperature decreased from 275° to 200°C, the average rate of temperature decrease would be 0.375°C/yr. For comparison, numerical modeling of the thermal history of a location above a cooling pluton that corresponds to the epithermal environment (Knapp and Norton, 1981) indicates that the temperature will decrease from about 275° to 200°C in about 135,000 years. This corresponds to a rate of temperature decrease of 5.5×10^{-4}°C/yr. Using these two rates of temperature change as limiting values, T_h would decrease by about 1°C every 3 to 1,800 years. The zoned nature of the sphalerite crystal suggests that the temperature and/or salinity may have varied during crystal formation at Creede. The small T_h variations in this shallow system, where deeper magmatic fluids are mixing with cooler meteoric fluids, may reflect these natural temperature fluctuations during crystallization of the sphalerite and trapping of the inclusions.

The duration of hydrothermal activity in porphyry deposits is estimated to be on the order of 5×10^4 to 5×10^5 years, although large porphyry copper deposits with multiple intrusions and fluid events may span several millions of years (Norton, 1978; Seedorff et al., 2005; Weis et al., 2012; Spencer et al., 2015). Early two-phase, vapor-rich FIAs from Bingham Canyon show T_h variations of approximately 10°C. The brine inclusions show minimum T_h variations of 2° to 3°C, with the majority around 20° to 30°C. The late fluids at Bingham Canyon show minimum T_h variations of approximately 3°C, with the majority showing variations of ~10°C (Fig. 7).

Norton (1978), Weis et al., (2012), and S. Becker (unpub. report, 2018) indicate that the temperature near the top of the pluton in the porphyry environment decreases from 500° to 300°C in about 70,000 years, corresponding to a cooling rate of 2.8×10^{-3}°C/yr. Thus, the observed temperature variations in FIAs at Bingham Canyon would require that individual FIAs formed over a period of 700 to 11,000 years. Because fractures in quartz are known from experimental studies to heal over periods of weeks to years at these temperatures, the ranges in T_h likely reflect short-lived temperature fluctuations during formation of the FIAs.

At the Meguma orogenic lode gold deposit (Kontak et al., 1990) the temperature decreased from about 450°C in the early stages of mineralization to about 300°C in the later stages. The amount of time corresponding to the temperature decrease from 450° to 300°C (and to form the deposit) is unknown, but the duration of mineralization in orogenic lode gold deposits is generally less than the uncertainty on the age determinations, which in the case of Meguma translates to about 5×10^6 years, from 375 to 370 Ma. If we assume that it took at least 10,000 years and less than 10,000,000 years for the temperature to decrease from 450° to 300°C and deposit the Meguma mineralization, the average temperature decrease would range from 0.015°C/yr to 1.5×10^{-5}°C/yr, recognizing that the rate of temperature change was likely discontinuous. At Meguma, the carbonic FIAs show minimum T_h variation within an FIA of about 3° to 4°C, with the majority around 6° to 12°C. The H_2O-NaCl inclusions show minimum T_h variations between 5° and 7°C, with the majority between 20° and 30°C (Fig. 8). Assuming a cooling rate of 0.015°C/yr (i.e., the mineralization formed in 10,000 yr), the observed ranges in T_h could be produced in 200 to 2,000 years or in 200,000 to 2,000,000 years (assuming that the entire mineralization event lasted 10,000,000 yr). As noted above, experimental studies by Brantley et al. (1990) show that cracks in quartz heal in less than one year at temperatures >300°C. Thus, it appears that temperature decrease cannot account for the complete range in T_h observed at Meguma.

Primary FIAs trapped in the dark growth zones of quartz crystals from the Marble Canyon pegmatite show large T_h variations of 18° and 28°C. The observed minimum T_h variation for the early secondary inclusions restricted to the core of the quartz is around 3°C with the majority between 5° and 10°C. The late secondary inclusions in the rim show minimum T_h variations in the range of 2° to 3°C, with the majority around 5° to 8°C (Fig. 9).

Numerical models of cooling pluton environments (Knapp and Norton, 1981) indicate that temperatures in the core of the pluton (~10 km) decrease from 600° to 400°C in about 100,000 years, corresponding to an average temperature decrease of about 2×10^{-3}°C/year. This, in turn, would require from 1,000 years (ΔT_h = 2°C) to 14,000 years (ΔT_h = 28°C) to produce the observed temperature variations if they were the result of temperature decrease alone. However, assuming that the depth of formation was ≈10 km, the temperature at trapping would have been about 500°C. At this temperature fractures in quartz would heal in a matter of days. Again, it does not appear that the observed variations in T_h in the Marble Canyon pegmatite are the result of temperature variation alone. It is unlikely that temperature variations during the formation of an FIA can explain the observed variations in T_h in most of the samples studied, but T_h of fluid inclusions also depends on the trapping pressure. Perhaps some or all the variation might be related to pressure fluctuations during FIA formation, at least in some environments. In the epithermal environment, it is well known that pressure fluctuates between nearly lithostatic and hydrostatic conditions as a result of repeated sealing and fracturing (Cooke and Simmons, 2000). Similarly, in the orogenic lode gold deposits, Robert et al. (1995) have shown that pressure fluctuations and concomitant phase separation (boiling) are often associated with gold deposition. Hydraulic fracturing and brecciation related to pressure are also common in the porphyry environment. Fractures in tight-gas sandstone reservoirs are common features, and many form during repeated overpressuring owing to gas generation within the low-permeability reservoirs. Fluid inclusions record the oscillating pressures during fracture cementation. Fournier (1985) also noted that quartz solubility decreases with decreasing pressure at constant temperature, and the effect is especially

significant at temperatures >340°C (see also Monecke et al., 2018). As a result, FIAs could form at constant temperature as quartz precipitates during a fracturing event that results in a lower pressure. Thus, in the epithermal, porphyry copper, lode gold, and tight-gas reservoirs in basin environments, at least some of the observed variation in T_h may be the result of pressure fluctuations during the formation of FIAs.

Roedder's rules state that a fluid inclusion must trap a single, homogeneous phase in order to provide information on the original trapping conditions and fluid composition. However, boiling or fluid immiscibility is common in many environments, including the epithermal, porphyry, and orogenic gold environments examined here. Bodnar et al. (1985a) quantitatively described the effect of trapping multiple fluid phases in the epithermal environment and showed that trapping of only a few volume percent vapor along with the liquid would result in T_h that was several tens of degrees higher than the trapping temperature. Similarly, Lecumberri-Sanchez et al. (2014) show that many fluid inclusions in the porphyry copper environment that homogenize by halite dissolution are the result of trapping halite along with liquid. Accordingly, we note that in our study of the Bingham Canyon deposit, FIAs composed of inclusions that homogenize by halite dissolution generally show the greatest variability in T_h in the deposit. We suggest that trapping of multiple phases may contribute to the wide range in T_h (more than several tens of degrees) observed in some FIAs in the epithermal, porphyry, and orogenic gold environments. Following FIA formation, inclusions will be exposed to varying pressure and temperature conditions during burial or exhumation, and the inclusions might reequilibrate to their new pressure-temperature environment (Bodnar, 2003b). This process can lead to a range in T_h in an FIA, because individual fluid inclusions within the same FIA might respond differently to changes in pressure and/or temperature. Several factors determine the likelihood that a fluid inclusion will reequilibrate, including the inclusion size and shape, the physical and chemical properties of the host mineral, fluid composition, and the pressure-temperature path followed by the host rock after the entrapment (Bodnar, 2003b). Inclusions are most likely to reequilibrate when the pressure-temperature path followed after trapping differs from the path defined by the isochore of the inclusions. The pressure-temperature path followed by the inclusions after trapping determines if the internal pressure in the inclusion exceeds or is less than the confining pressure, resulting in different diagnostic textures for the fluid inclusions (Vityk et al., 1994, 2000; Bodnar, 2003b). As the inclusion volume or composition changes, the microthermometric behavior of inclusions changes accordingly. When the mineral follows a pressure-temperature path that results in an internal overpressure in the inclusions, the volume of the inclusions can increase by stretching, thus decreasing the density in the fluid and resulting in an increase in the T_h. As larger inclusions are more susceptible to internal overpressure, these inclusions will reequilibrate to the largest extent, resulting in higher T_h and leading to variations in T_h within an FIA.

The physical and chemical properties of the host mineral affect the extent to which a given fluid inclusion will respond to changing pressure-temperature conditions following trapping. Fluid inclusions in soft cleavable minerals (fluorite, sphalerite, and barite) are more likely to stretch and leak if the inclusions are overheated in nature or in laboratory (Bodnar and Bethke, 1984; Ulrich and Bodnar, 1988), while fluid inclusions in hard minerals, such as quartz, are more likely to withstand the increase in internal pressure and maintain their original shape, volume, and fluid content (Bodnar, 2003b).

A textbook example of the effect of stretching on fluid inclusions in nature was observed in quartz from the Meguma metamorphic lode-gold deposit. Thirty-eight fluid inclusions, containing a low-salinity H_2O-NaCl solution and located along a healed fracture (15 of the 38 inclusions are shown on Fig. 16a) have similar sizes and apparently similar liquid-to-vapor ratios at room temperature. These inclusions clearly represent an FIA and were trapped at the same time, and one would expect them to show similar T_h. However, the inclusions show a wide range in T_h, from 163.3° to 288°C (Figs. 8, 16b). The distribution of T_h for this FIA is similar to that shown by both natural and synthetic fluid inclusions that have reequilibrated by stretching. Vityk and Bodnar (1995) trapped fluid inclusions in natural quartz at 700°C and 500 MPa and then reequilibrated the inclusions at 625°C and 200 MPa for a period of 180 days such that the internal pressure in the inclusions at the reequilibration conditions was higher than the confining pressure in the autoclave (200 MPa). Fluid inclusions that originally homogenized at ~284°C subsequently homogenized between 305° and 330°C, and one homogenized at 372°C, all as a result of stretching (Fig. 16c). Comparing the histogram for the Meguma FIA with the experimental results shows similarities in the distribution of T_h (Fig. 16b, c). The comparison suggests that the wide range in T_h observed in the Meguma FIA is a result of stretching. This observation is important when interpreting these data because the lowest T_h (highest density) most closely represents the original trapping conditions. In many fluid inclusion studies in which T_h distributions similar to those shown in Figure 16b and c are reported, the authors selected the average T_h (i.e., ≈220°C at Meguma and ≈315°C in the experimental sample) as most closely representing the original trapping conditions; this interpretation is clearly incorrect. Another common process that can lead to variations in T_h is necking down of fluid inclusions (Roedder, 1984) that occurs as a result of dissolution and reprecipitation of the host mineral. Necking down is most commonly associated with secondary fluid inclusions formed along healed microfractures (Roedder, 1962). However, it is important to emphasize that all inclusions tend to become more regularly shaped with time and may evolve into several smaller inclusions following trapping. If necking of the inclusions occurs at the pressure-temperature trapping conditions or in a closed (isochoric) system in the one-phase fluid field, the inclusions will all have similar phase ratios and microthermometric behavior; this would not affect the T_h of the inclusion. If the inclusion does not remain an isochoric system during necking, or if necking occurs in the presence of two or more phases, the inclusions will likely show a range in microthermometric data. Similarly, if necking occurs over a range of pressure-temperature conditions and under nonisochoric conditions, a range in T_h will result. For example, a density variation of about 5% could produce T_h variations within the FIA of at least 50°C in the diagenetic environment (Goldstein and Reynolds, 1994).

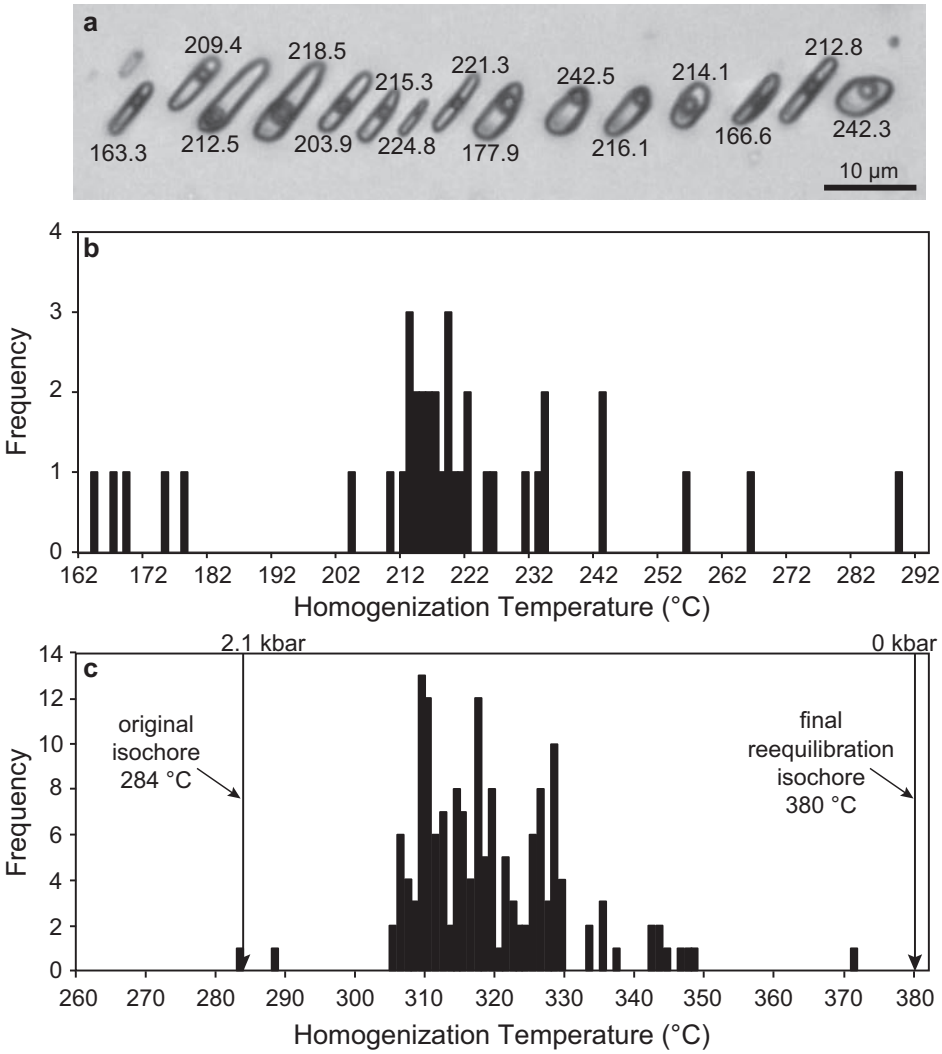

Fig. 16. Effect of stretching on the homogenization temperature (T_h) variation of a fluid inclusion assemblage (FIA) in quartz from the orogenic lode gold deposit of the Meguma metamorphic terrane, Nova Scotia, Canada. (a) Photomicrograph of the FIA showing similarly sized and shaped fluid inclusions; the numbers represent homogenization temperatures for the individual inclusions in the FIA. (b) Histogram showing the distribution of homogenization temperatures within the FIA. (c) Histogram showing the distribution of homogenization temperatures for synthetic fluid inclusions that have reequilibrated by stretching at 625°C and 200 MPa after 180 days (after Vityk and Bodnar, 1995).

Variations associated with sampling, sample preparation, and data collection: The environment from which the sample is collected and the methods employed during sample collection could also produce ranges in T_h in some FIAs. During core drilling, drill core temperatures may reach 110° to 230°C (Goldstein and Reynolds, 1994), and low-temperature fluid inclusions could be overheated during drilling. Also, samples collected during drilling may be dried in an oven before being stored, and the fluid inclusion may be heated to temperatures well above T_h. Fluid inclusions in outcrop samples can also be overheated by solar heating or by forest or grass fires. Fluid inclusions in samples collected from the surface in areas that experience annual freeze cycles, including locations at high latitude or high elevation, could experience freeze stretching, as described in more detail below. Samples that might have seen any of these conditions should be avoided as the inclusions may have reequilibrated to produce elevated T_h values.

Thermal or structural damage to the sample can also be introduced during cutting, grinding, and polishing of the thick sections, leading to anomalous T_h values. Also, if the sample has been heated to cure the cement used to mount the sample on a glass slide, inclusions may be damaged. Today, most inclusionists are aware of these issues and take care to avoid damage to the sample during preparation, but some older data in the literature may have been affected by poor sample preparation protocols. As noted above, if fluid inclusions are subjected to conditions such that the internal pressure in the inclusion exceeds the confining pressure, the fluid inclusions may reequilibrate through stretching, leakage, or decrepitation (Bodnar, 2003b). This may occur in nature following inclusion trapping but can also occur during

microthermometric analysis in the lab. During heating from room temperature, the pressure in the fluid inclusion will increase and could lead to nonelastic volume changes to the inclusion and/or loss of material from the inclusion; in both cases a higher T_h will result. To minimize the likelihood that fluid inclusions will reequilibrate during heating in the lab and to increase the probability that reequilibration will be recognized, data should only be collected from any fluid inclusion during the first, and only, heating run to measure the T_h. This approach will avoid the possibility of overheating (and possibly modifying) an inclusion before its T_h is measured. Aqueous fluid inclusions that homogenize at low temperature may also reequilibrate during cooling to measure the ice-melting temperature. The volume of the ice phase that forms when the liquid freezes is 9.06% larger than that of the liquid. As such, if the vapor bubble in the inclusion occupies less than 9.06 vol % of the inclusion before freezing, the ice will expand to fill the entire inclusion volume and push on the inclusion walls to generate high pressures that can stretch the inclusions (Lawler and Crawford, 1983). A pure H_2O inclusion containing 9.06 vol % vapor at the pure H_2O triple point (0.01°C) (or 8.9 vol % vapor at 22°C) will homogenize at 158°C; thus, any aqueous fluid inclusion that homogenizes at ≤150°C may stretch during freezing. Therefore, the T_h of low-temperature inclusions should be measured before the ice-melting temperature is measured. In this study, all freezing measurements were made after T_h was measured, so freeze stretching could not be the cause of T_h variations observed in this study. Even in the ideal situation in which every fluid inclusion in the FIA is trapped at exactly the same temperature and pressure, the T_h of the inclusions would still show a small variation that is related to the size of the fluid inclusion (Fall et al., 2009). As inclusions are heated, the vapor bubble shrinks and reaches a critical bubble radius at which point the bubble will "blink out," i.e., the inclusion will homogenize to the liquid phase. Thus, within the same FIA small fluid inclusions would homogenize at slightly lower temperature than larger inclusions. This behavior is largely a function of the surface tension of the liquid-vapor interface and the radius of the vapor bubble. For aqueous inclusions that homogenize at temperatures less than about 230°C, the maximum range in T_h resulting from variations in inclusion size should be no more than a few degrees. The size dependency of T_h decreases with increasing temperature, and for aqueous inclusions the size effect is not observed for T_h higher than about 230°C. This is expected as the surface tension decreases with increasing temperature and becomes nil at the critical point (Fall et al., 2009).

Primary versus secondary origin of fluid inclusions

Microthermometric data collected for this study reveal a systematic difference in ranges of T_h of FIAs consisting of primary fluid inclusions compared to those composed of secondary fluid inclusions. This difference is perhaps best illustrated by the data from the Cave-in-Rock MVT deposit (Fig. 6), where the average range in T_h of FIAs containing cubic primary inclusions is 5.8°C, the average range in T_h of FIAs containing irregularly shaped primary inclusions is 7.7°C, and the average range in T_h of FIAs containing secondary inclusions is 2.1°C. In the case of primary fluid inclusions, the fluid event is represented by formation of a growth zone in a crystal, whereas secondary fluid inclusions represent the healing of a microfracture. Thus, based on experimental data that document that cracks in most minerals heal almost instantaneously on a geologic time scale (days to months to a few years, depending on the PTX conditions), it is not surprising that secondary FIAs show a smaller range in T_h compared to primary FIAs. We note, however, that in some cases, such as the Creede sphalerite example, 15 out of 20 primary FIAs show ranges of ≤3°C.

Is the range in T_h within FIAs related to the number of fluid inclusions measured and T_h?

One might expect that as the number of fluid inclusions within an FIA that are measured increases, the range in T_h for that FIA would increase. However, in this study, only a weak correlation is observed between the range in T_h within an FIA and the number of inclusions measured (Fig. 17). As an example, 56 fluid inclusions from a single FIA in fluorite from the Cave-in-Rock district were measured, and the total range in T_h was less than 3°C (Fig. 6). Conversely, some FIAs in other environments in which fewer than 10 fluid inclusions were measured show ranges >100°C (cf. Figs. 7–9). In other cases, FIAs in which several tens of fluid inclusions were measured often show ranges of <20° to 30°C (Figs. 6, 7b, 8, 9).

One might also expect that FIAs with higher T_h might show larger ranges within FIAs. Our data show a slight correlation between the observed range in T_h in a given FIA and the average T_h of the FIA (Fig. 18); this is not unexpected as fluid inclusions trapped at higher temperature likely experienced a wider range in temperature (and pressure) conditions following formation, thus increasing the probability of reequilibration.

Summary of Results

Homogenization temperatures of fluid inclusions from well-constrained FIAs from several different environments were

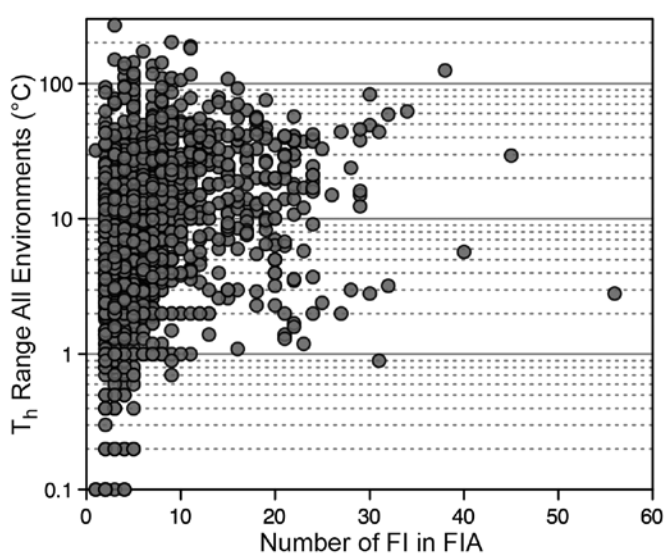

Fig. 17. Total range in homogenization temperature (T_h) within individual fluid inclusion assemblages (FIAs) shown on a log scale for all samples examined in this study, including those data collected in the present study and those reported in the literature (Table 2), plotted as a function of the number of fluid inclusions (FIs) measured in each FIA.

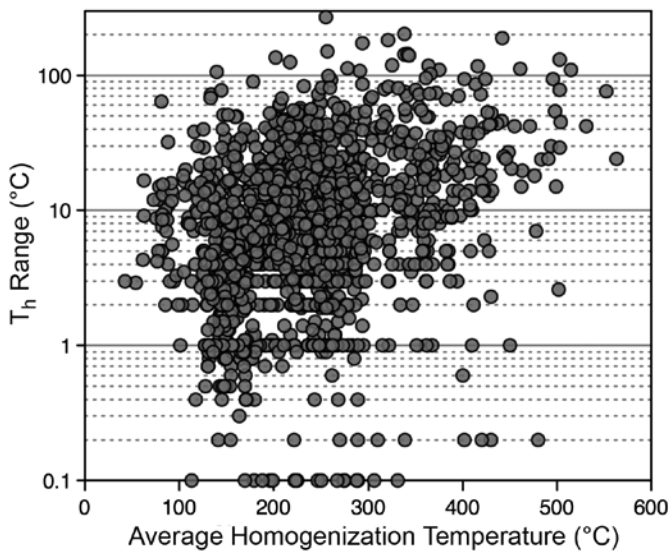

Fig. 18. Total range in homogenization temperature (T_h) within individual fluid inclusion assemblages (FIAs) shown on a log scale for all samples examined in this study, including those data collected in the present study and those reported in the literature (Table 2), plotted as a function of the average T_h of each FIA.

measured in this study to characterize the range in T_h for individual FIAs. These data were combined with vetted data from the literature, and the ranges in T_h within individual FIAs that could be expected in different environments was determined. Fluid inclusion assemblages in all environments studied show at least a few FIAs with variations ≤1°C, and all environments also show FIAs with ranges of several tens of degrees or more. Approximately 1,700 FIAs from all environments were considered (Fig. 19a). Of these, approximately 50% of all FIAs show a range in T_h of ≤10°C, and ~80% of all FIAs show a range ≤20°C (Fig. 19b). These data suggest that the temperature of an individual fluid event, such as healing of a microfracture or formation of a growth zone in a crystal, can be constrained to within a few tens of degrees with careful selection of well-constrained FIAs.

In deep, low-permeability sedimentary environments analogous to tight-gas sandstones studied here, the temperature of a fluid event exhibited by a single crack-sealing feature can be determined to within ±0.5°C in about one-third of the cases, and the median range in T_h for all 144 FIAs considered is 2°C, with a range from 2.7°C (Q1) to 3.7°C (Q3) (Figs. 10, 20).

Data from 116 FIAs from MVT deposits show a median range in T_h of 4.1°C, with a range from 2.3°C (Q1) to 8.3°C (Q3), indicating that it is generally possible to constrain the temperature of a fluid event in MVT environments to better than ~4°C. In 31 out of 116 FIAs the range in T_h was <2°C (Figs. 11, 20).

Analysis of the data for epithermal deposits shows that 102 out of 923 FIAs show a range of 1°C or less. The median range in T_h for all 923 FIAs considered is 9°C, with a range from 3.8°C (Q1) to 19°C (Q3). Data from the Creede sphalerite show that the temperature of formation of 15 of the 20 individual growth zones can be determined to within 3°C (Fig. 5a; Table 1).

Analysis of the data for porphyry deposits shows that 24 out of 271 FIAs have a range of 1°C or less. The median range in

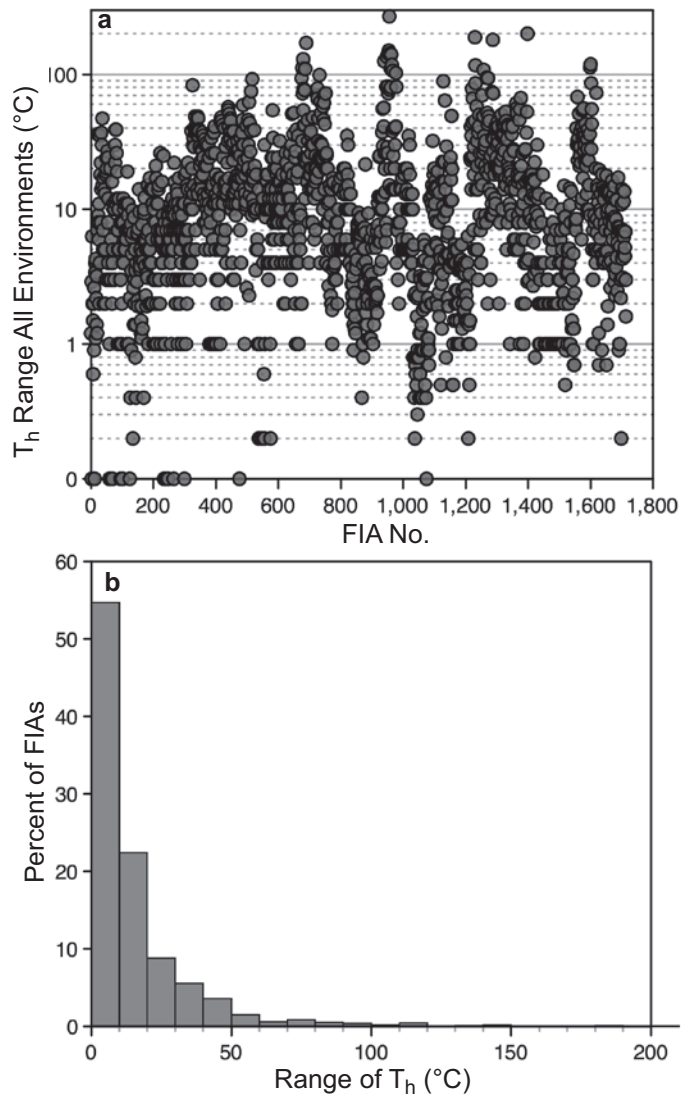

Fig. 19. (a) Total range in homogenization temperature (T_h) within individual fluid inclusion assemblages (FIAs) shown on a log scale for all samples examined in this study, including those data collected in the present study and those reported in the literature (Table 2). (b) Histogram showing the frequency of the total range in homogenization temperature (T_h) within individual FIAs for all samples examined in this study, including those data collected in the present study and those reported in the literature (Table 2). Note that ~80% of all FIAs show ≤20°C variation within individual FIAs.

T_h for all 271 FIAs considered is 15°C, with a range from 8°C (Q1) to 30°C (Q3) (Figs. 13, 20). These data suggest that a range in T_h of ~15°C is an achievable goal during microthermometric studies of intrusion-related magmatic hydrothermal systems.

Data for orogenic gold deposits show that 21 out of 231 FIAs have a range of 1°C or less. The median range in T_h for all 231 FIAs considered is 8.7°C, with a range from 4°C (Q1) to 20°C (Q3) (Figs. 14, 20). Our results suggest that the temperature of a fluid event in orogenic gold systems can be constrained to within ~9°C (the median range).

Too few data are available for pegmatites, intrusion-related gold deposits and skarn deposits to offer defensible

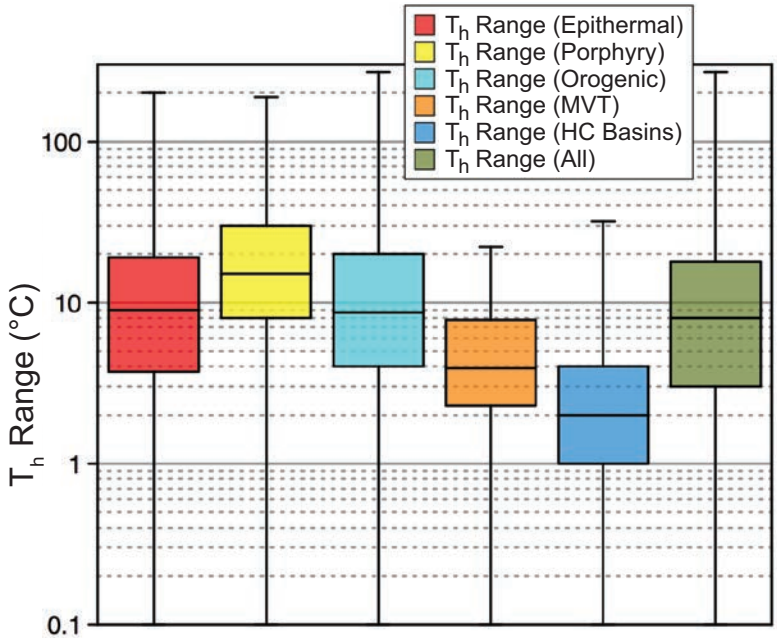

Fig. 20. Box and whisker plots showing the range in homogenization temperature (T_h) on a log scale within individual fluid inclusion assemblages sorted according to geologic environment and other characteristics. Shown are the complete range in observed T_h ranges, the 25th and 75th percentiles of the ranges, and the median range for a given environment. Position along the x-axis is arbitrary and is arranged approximately according to the scatter in observed T_h range. MVT = Mississippi Valley-type.

recommendations concerning achievable ranges in T_h for these environments.

Acknowledgments

We would like to thank Csaba Szabó, J. Donald Rimstidt, Robert Lowell, and Robert Tracy for their constructive comments on an earlier version of the manuscript; Charles Farley for technical support; and Dan Kontak, Jim Student, Paul Spry, and the Fracture Research and Application Consortium at the Bureau of Economic Geology for providing samples and data for the study. Numerous discussions with Jim Reynolds have helped us to focus and refine our approach and to eliminate much of the ambiguity that was present in earlier versions of this manuscript. Financial support was provided by U.S. National Science Foundation under grant EAR 1624589 to RJB. Partial financial support was provided by grant DE-FG02-03ER15430 from Chemical Sciences, Geosciences and Biosciences Division, Office of Basic Energy Sciences, Office of Science, U.S. Department of Energy, and by the Career-Development Publication Award and industrial sponsors of the Fracture Research and Application Consortium at the Bureau of Economic Geology, Jackson School of Geosciences, University of Texas Austin, to AF.

REFERENCES

Alzayer, Y., Eichhubl, P., and Laubach, S.E., 2015, Non-linear growth kinematics of opening-mode fractures: Journal of Structural Geology, v. 74, p. 31–44.

Anderson, E.D., Atkinson Jr., W.W., Marsh, T., and Iriondo, A., 2009, Geology and geochemistry of the Mammoth breccia pipe, Copper Creek mining district: Evidence for a magmatic-hydrothermal origin: Mineralium Deposita, v. 44, p. 151–170.

Audétat, A., 1999, The magmatic-hydrothermal evolution of the Sn/W-mineralized Mole granite (Eastern Australia): Ph.D. dissertation, Zürich, ETH Zürich, 210 p.

Audétat, A., Günther, D., and Heinrich, C.A., 2000, Magmatic-hydrothermal evolution in a fractionating granite: A microchemical study of the Sn-W-F–mineralized Mole granite (Australia): Geochimica et Cosmochimica Acta, v. 64, p. 3373–3393.

Barton, P.B., Bethke, P.M., and Roedder, E., 1977, Environment of ore deposition in the Creede mining district, San Juan Mountains, Colorado: III. Progress toward interpretation of the chemistry of the ore-forming fluid for the OH vein: Economic Geology, v. 72, p. 1–24.

Beane, R.E., and Bodnar, R.J., 1995, Hydrothermal fluids and hydrothermal alteration in porphyry copper deposits: Arizona Geological Society Digest, v. 20, p. 83–93.

Becker, S.P., Eichhubl, P., Laubach, S.E., Reed, R.M., Lander, R.H., and Bodnar, R.J., 2010, A 48 m.y. history of fracture opening, temperature, and fluid pressure: Cretaceous Travis Peak Formation, East Texas basin: Geological Society of America Bulletin, v. 122, p. 1081–1093.

Berni, G.V., Heinrich, C.A., Lobato, L.M., and Wall, V., 2016, Ore mineralogy of the Sierra Pelada Au-Pd-Pt deposit, Carajás, Brazil, and implications for ore-forming processes: Mineralium Deposita, v. 51, p. 781–795.

Bethke, P.M., and Rye, R.O., 1979, Environment of ore deposition in the Creede mining district, San Juan Mountains, Colorado: IV. Source of fluids from oxygen hydrogen, and carbon isotopic studies: Economic Geology, v. 74, p. 1832–1851.

Bethke, P.M., Barton, P.B., Lanphere, M.A., and Steven, T.A., 1976, Environment of ore deposition in the Creede mining district, San Juan Mountains, Colorado: II. Age of mineralization: Economic Geology, v. 71, p. 1006–1011.

Bierlein, F.P., and Crowe, D.E., 2000, Phanerozoic orogenic lode gold deposits: Reviews in Economic Geology, v. 13, p. 103–139.

Bodnar, R.J., 1994, Synthetic fluid inclusions. XII. Experimental determination of the liquidus and isochores for a 40 wt % H_2O-NaCl solution: Geochimica et Cosmochimica Acta, v. 58, p. 1053–1063.

——1995, Fluid inclusion evidence for magmatic source for metals in porphyry copper deposits: Mineralogical Association of Canada Short Course, v. 23, p. 139–152.

——2003a, Introduction to fluid inclusions: Mineralogical Association of Canada Short Course, v. 32, p. 81–99.

——2003b, Reequilibration of fluid inclusions: Mineralogical Association of Canada Short Course, v. 32, p. 213–231.

Bodnar, R.J., and Bethke, P.M., 1984, Systematics of stretching of fluid inclusions; I: Fluorite and sphalerite at 1 atmosphere confining pressure: Economic Geology, v. 79, p. 141–161.

Bodnar, R.J., and Sterner, S.M., 1985, Synthetic fluid inclusions in natural quartz. II. Application to PVT studies: Geochimica et Cosmochimica Acta, v. 49, p. 1855–1859.

Bodnar, R.J., and Vityk, M.O., 1994, Interpretation of microthermometric data from H_2O-NaCl fluid inclusions, *in* De Vivo, B., and Frezzotti, M.L., eds., Fluid inclusions in minerals: Methods and applications: Blacksburg, Virginia, Virginia Tech, p. 117–130.

Bodnar, R.J., Reynolds, T.J., and Kuehn, C.A., 1985a, Fluid inclusion systematics in epithermal systems: Reviews in Economic Geology, v. 2, p. 73–98.

Bodnar, R.J., Burnham, C.W., and Sterner, S.M., 1985b, Synthetic fluid inclusions in natural quartz. III. Determination of phase equilibrium properties in the system H_2O-NaCl to 1,000°C and 1,500 bars: Geochimica et Cosmochimica Acta, v. 49, p. 1861–1873.

Brantley, S.L., 1992, The effect of fluid chemistry on quartz microcrack lifetimes: Earth and Planetary Science Letters, v. 113, p. 145–156.

Brantley, S.L., Evans, B., Hickman, S.H., and Crerar, D.A., 1990, Healing of microcracks in quartz: Implication for fluid flow: Geology, v. 18, p. 136–139.

Brathwaite, R.L., and Faure, K., 2002, The Waihi epithermal gold-silver-base metal sulfide-quartz vein system, New Zealand: Temperature and salinity controls on electrum and sulfide deposition: Economic Geology, v. 97, p. 269–290.

Brown, C.A., Smagala, T.M., and Haefele, G.R., 1986, Southern Piceance basin model— Cozzette, Corcoran, and Rollins sandstones: American Association of Petroleum Geologists (AAPG) Studies in Geology, v. 24, p. 207–219.

Browne, P.R.L., Courtney, S.F., and Wood, C.P., 1989, Formation rates of calc-silicate minerals deposited inside drilling casing, Ngatamariki geothermal field, New Zealand: American Mineralogist, v. 74, p. 759–763.

Campbell, W.R., and Barton, P.B., 2005, Environment of ore deposition in the Creede mining district, San Juan Mountains, Colorado: Part VI: Maximum duration for mineralization of the OH vein: Economic Geology, v. 100, p. 1313–1324.

Catchpole, H., Kouzmanov, K., Putlitz, B., Seo, J.H., and Fontboté, L., 2015, Zoned base metal mineralization in a porphyry system: Origin and evolution of mineralizing fluids in the Morococha district, Peru: Economic Geology, v. 110, p. 39–71.

Černý, P., 1991, Rare-element granitic pegmatites. Part 1: Anatomy and internal evolution of pegmatite deposits. Part 2: Regional to global environments and petrogenesis: Geoscience Canada, v. 18, p. 49–81.

Černý, P., and Ercit, T.S., 2005, Classification of granitic pegmatites revisited: Canadian Mineralogist, v. 43, p. 2005–2026.

Chinchilla, D., Ortega, L., Piña, R., Merinero, R., Lunar, R., Moncada, D., and Bodnar, R.J., 2015, Fluid evolution in the Patricia Zn-Pb-Ag vein deposit (Paguanta, NE Chile): Fluid inclusion assemblages and laser ablation ICP-MS evidence: Society for Geology Applied to Mineral Deposits (SGA) Biennial Meeting, 13th, Nancy, France, August 24–27, 2015, Proceedings, 4 p.

Cline, J.S., and Bodnar, R.J., 1994, Direct evolution of brine from a crystallizing silicic melt in the Questa, New Mexico, molybdenum deposit: Economic Geology, v. 89, p. 1780–1802.

Coleman, D.S., Bartley, J.M., Glazner, A.F., and Law, R.D., 2005, Incremental assembly and emplacement of Mesozoic plutons in the Sierra Nevada and White and Inyo ranges, California: Rethinking the Assembly and Evolution of Plutons: Field Tests and Perspectives: Geological Society of America Field Forum, Sierra Nevada and White and Inyo ranges, California, October 7–14, 2005, Field Trip Guide, 51 p.

Cooke, D.R., and Simmons, S.F., 2000, Characteristics of epithermal gold deposits: Reviews in Economic Geology, v. 13, p. 221–244.

Cumella, S.P., and Scheevel, J., 2008, The influence of stratigraphy and rock mechanics on Mesaverde gas distribution, Piceance basin, Colorado: American Association of Petroleum Geologists (AAPG) Hedberg Series, v. 3, p. 137–155.

Diamond, L.W., 1990, Fluid inclusions evidence for P-V-T-X evolution of hydrothermal solutions in late-alpine gold-quartz veins at Brusson, Val D'Ayas, northwest Italian Alps: American Journal of Science, v. 290, p. 912–958.

Eichhubl, P., and Boles, J.R., 2000, Rates of fluid flow in fault systems—evidence for episodic rapid fluid flow in the Miocene Monterey Formation, coastal California: American Journal of Science, v. 300, p. 571–600.

Estrade, G., Salvi, S, Beziat, D., and Williams-Jones, A.E., 2015, The origin of skarn-hosted rare-metal mineralization in the Ambohimirahavavy alkaline complex, Madagascar: Economic Geology, v. 110, p. 1485–1513.

Fall, A., Rimstidt, J.D., and Bodnar, R.J., 2009, The effect of fluid inclusion size on determination of homogenization temperature and density of liquid-rich aqueous inclusions: American Mineralogist, v. 94, p. 1569–1579.

Fall, A., Eichhubl, P., Cumella, S.P., Bodnar, R.J., Laubach, S.E., and Becker, S.P., 2012, Testing the basin-centered gas accumulation model using fluid inclusion observations: Southern Piceance basin, Colorado: American Association of Petroleum Geologists (AAPG) Bulletin, v. 96, p. 2297–2318.

Fall, A., Eichhubl, P., Bodnar, R.J., Laubach, S.E., and Davis, J.S., 2015, Natural hydraulic fracturing of tight-gas sandstone reservoirs, Piceance basin, Colorado: Geological Society of America Bulletin, v. 127, p. 61–75.

Fall, A., Ukar, E., and Laubach, S.E., 2016, Origin and timing of Dauphiné twins in quartz cement in fractured sandstones from diagenetic environments: Insight from fluid inclusions: Tectonophysics, v. 687, p. 195–209.

Fonarev, V.I., Touret, J.L.R., and Kotelnikova, Z.A., 1998, Fluid inclusions in rocks from the Central Kola granulite area, Baltic Shield: European Journal of Mineralogy, v. 10, p. 1181–1200.

Fournier, R.O., 1985, The behavior of silica in hydrothermal solutions: Reviews in Economic Geology, v. 2, p. 45–62.

Garven, G., and Raffensperger, J.P., 1997, Hydrology and geochemistry of ore genesis in sedimentary basins, *in* Barnes, H.L., ed., Geochemistry of hydrothermal ore deposits: New York, Wiley, p. 125–189.

Goldstein, R.H., 2003, Petrographic analysis of fluid inclusions: Mineralogical Association Canada Short Course, v. 32, p. 9–53.

Goldstein, R.H., and Reynolds, T.J., 1994, Systematics of fluid inclusions in diagenetic minerals: Society of Sedimentary Geologists (SEPM) Short Course, v. 31, 199 p.

Hayba, D.O., 1997, Environment of ore deposition in the Creede mining district, San Juan Mountains, Colorado: Part V. Epithermal mineralization from fluid mixing in the OH vein: Economic Geology, v. 92, p. 29–44.

Hollister, L.S., Crawford, M.L., Roedder, E., Burruss, R.C., Spooner, E.T.C., and Touret, J., 1981, Practical aspects of microthermometry: Mineralogical Association of Canada Short Course, v. 6, p. 13–38.

Jackson, J.L., Matty, D.J., Reynolds, B.A., Chandonais, D.R., and Student, J.J., 2007, Petrology and geochemistry of the Eureka Valley monzonite, White-Inyo mountains, California: Geological Society of America Abstracts with Program, v. 39, p. 318.

Johnson, R.C., 1989, Geologic history and hydrocarbon potential of Late Cretaceous-age, low-permeability reservoirs, Piceance basin, western Colorado: U.S. Geological Survey Bulletin 1787-E, 51 p.

Kendrick, M.A., Burgess, R., Leach, D., and Pattrick, R.A.D., 2002, Hydrothermal fluid origins in Mississippi Valley-type ore districts: Combined noble gas (He, Ar, K) and halogen (Cl, Br, I) analysis of fluid inclusions from the Illinois-Kentucky fluorspar district, Viburnum trend, and Tri-State districts, Midcontinent United States: Economic Geology, v. 97, p. 453–469.

Klein, E.L., Ribeiro, J.W.A., Harris, C., Moura, C.A.V., and Giret, A., 2008, Geology and fluid characteristics of the Mina Velha and Mandiocal orebodies and implications for the genesis of the orogenic Chega Tudo gold deposit, Gurupi belt, Brazil: Economic Geology, v. 103, p. 957–980.

Klemm, L.M., Pettke, T., Hienrich, C.A., and Campos, E., 2007, Hydrothermal evolution of the El Teniente deposit, Chile: Porphyry Cu-Mo ore deposition from low-salinity magmatic fluids: Economic Geology, v. 102, p. 1021–1045.

Klemm, L.M., Pettke, T., and Heinrich, C.A., 2008, Fluid and source magma evolution of the Questa porphyry Mo deposit, New Mexico, USA: Mineralium Deposita, v. 43, p. 533–552.

Knapp, R.B., and Norton, D., 1981, Preliminary numerical analysis of processes related to magma crystallization and stress evolution in cooling pluton environments: American Journal of Science, v. 281, p. 35–68.

Kontak, D.J., and Kerrich, R., 2002, An isotopic (C, O, Sr) study of vein gold deposits in the Meguma Terrane, Nova Scotia; implication for source reservoirs: Economic Geology, v. 92, p. 161–180.

Kontak, D.J., and Kyser, K., 2011, A fluid inclusion and isotopic study of an intrusion-related gold deposit (IRGD) setting in the 380 Ma South Mountain batholith, Nova Scotia, Canada: Evidence for multiple fluid reservoirs: Mineralium Deposita, v. 46, p. 337–363.

Kontak, D.J., Smith, P.K., Kerrich, R., and Williams, P.F., 1990, Integrated model for Meguma Group lode gold deposits, Nova Scotia, Canada: Geology, v. 18, p. 238–242.

Kontak, D.J., Horne, R.J., and Smith, P.K., 2001, Meguma gold deposits, Nova Scotia: Overview of past work with implications for future work: Geological Association of Canada, Mineral Deposits Division Newsletter, v. 71, p. 1–9.

——2005, Meguma gold deposits of Nova Scotia: Complexities of mesothermal, sediment-hosted gold mineralization revealed: Geological Association of Canada, Newfoundland Section, Atlantic Geology, v. 41, p. 181.

Kontak, D.J., Horne, R.J., and Kyser, K., 2011, A stable isotope ($\delta^{18}O$) study of two saddle-reef vein systems, Meguma gold fields, Nova Scotia, Canada: Evidence for similar isotopic signatures for different age deposits and regional implications: Mineralium Deposita, v. 46, 289–304.

Lander, R.H., and Laubach, S.E., 2015, Insights into rates of fracture growth and sealing from a model for quartz cementation in fractured sandstones: Geological Society of America Bulletin, v. 127, p. 516–538.

Landtwing, M.R., Pettke, T., Halter, W.E., Heinrich, C.A., Redmond, P.B., Einaudi, M.T., and Kunze, K., 2005, Copper deposition during quartz dissolution by cooling magmatic-hydrothermal fluids: The Bingham porphyry: Earth and Planetary Science Letters, v. 235, p. 229–243.

Landtwing, M.R., Furrer, C., Redmond, P.B., Pettke, T., Guillong, M., and Heinrich, C.A., 2010, The Bingham Canyon Cu-Mo-Au deposit. III. Zoned copper-gold ore deposition by magmatic vapor expansion: Economic Geology, v. 105, p. 91–118.

Laubach, S.E., Lander, R.H., Bonnell, L.M., Olson, J.E., and Reed, R.M., 2004, Opening histories of fractures in sandstone: Geological Society of London Special Publications, v. 231, p. 1–9.

Laubach, S.E., Fall, A., Copley, L.K., Marrett, R., and Wilkins, S.J., 2016, Fracture porosity creation and persistence in a basement-involved Laramide fold, Upper Cretaceous Frontier Formation, Green River basin, USA: Geological Magazine, v. 153, p. 887–910.

Law, B.E., 2002, Basin-centered gas systems: American Association of Petroleum Geologists (AAPG) Bulletin, v. 86, p. 1891–1919.

Lawler, J.P., and Crawford, M.L., 1983, Stretching of fluid inclusions resulting from a low-temperature microthermometric technique: Economic Geology, v. 78, p. 527–529.

Leach, D.L., and Sangster, D.F., 1993, Mississippi Valley-type lead-zinc deposits: Geological Association of Canada Special Paper 40, p. 289–314.

Leach, D.L., Bradley, D., Lewchuk, M.T., Symons, D.T.A., de Marsily, G., and Brannon, J., 2001, Mississippi Valley-type lead-zinc deposits through geological time: Implications from recent age-dating research: Mineralium Deposita, v. 36, p. 711–740.

Leach, D.L., Sangster, D.F., Kelley, K.D., Large, R.R., Garven, G., Allen, C.R., Gutzmer, J., and Walters, S., 2005, Sediment hosted lead-zinc deposits: A global perspective: Economic Geology 100th Anniversary Volume, p. 561–607.

Lecumberri-Sanchez, P., Romer, R.L., Lüders, V., and Bodnar, R.J., 2014, Genetic relationship between silver-lead-zinc mineralization in the Wutong deposit, Giangxi Province and Mesozoic granitic magmatism in the Nanling belt, southeast China: Mineralium Deposita, v. 49, p. 353–369.

LeFort, D., Hanley, J., and Guillong, M., 2011, Subepithermal Au-Pd mineralization associated with an alkalic porphyry Cu-Au deposit, Mount Milligan, Quesnel terrane, British Columbia, Canada: Economic Geology, v. 106, p. 781–808.

Lesage, G., Richards, J.P., Muehlenbachs, K., and Spell, T.L., 2013, Geochronology, geochemistry, and fluid characterization of the Late Miocene Buriticá gold deposit, Antioquia Department, Colombia: Economic Geology, v. 108, p. 1067–1097.

Lin, F., and Bodnar, R.J., 2010, Synthetic fluid inclusions XVIII: Experimental determination of the PVTX properties of H_2O-CH_4 to 500°C and $X_{CH4} \leq 4$ mol %: Geochimica et Cosmochimica Acta, v. 74, p. 3260–3273.

Márquez-Zavalía, M.F., and Heinrich, C.A., 2016, Fluid evolution in a volcanic-hosted epithermal carbonate-base metal-gold vein system Alto de la Blenda, Farallón Negro, Argentina: Mineralium Deposita, v. 51, p. 873–902.

Marshall, D., Downes, P.J., Ellis, S., Greene, R., Loughrey, L., and Jones, P., 2016, Pressure-temperature-fluid constraints for the Poona emerald deposits, Western Australia: Fluid inclusion and stable isotope studies: Minerals, v. 6, 22 p.

Maydagán, L., Franchini, M., Rusk, B., Lentz, D.R., McFarlane, C., Impiccini, A., Rios, F.J., and Rey, R., 2015, Porphyry to epithermal transition in the Altar Cu-(Au-Mo) deposit, Argentina, studied by cathodoluminescence, LA-ICP-MS, and fluid inclusion analysis: Economic Geology, v. 110, p. 889–923.

McMillan, W.J., and Pantaleyev, A., 1988, Porphyry copper deposits, *in* Roberts, R.G., and Sheehan, P.A., eds., Ore deposit models: Geological Association of Canada, Geoscience Canada Reprint Series, v. 3, p. 45–58.

Meinert, L.D., Hefton, K.K., Mayes, D., and Tasiran, I., 1997, Geology, zonation, and fluid evolution of the Big Gossan Cu-Au skarn deposit, Ertsberg district, Irian Jaya: Economic Geology, v. 92, p. 509–534.

Miron, G.D., Wagner, T., Wälle, M., and Heinrich, C.A., 2013, Major and trace-element composition and pressure-temperature evolution of rock-buffered fluids in low-grade accretionary-wedge metasediments, Central Alps: Contributions to Mineralogy and Petrology, v. 165, p. 981–1008.

Moncada, D., and Bodnar, R.J., 2012, Gangue mineral textures and fluid inclusion characteristics of the Santa Margarita Vein in the Guanajuato mining district, Mexico: Central European Journal of Geosciences, v. 4, p. 300–309.

Moncada, D., Baker, D., and Bodnar, R.J., 2017, Mineralogical, petrographic, and fluid inclusion evidence for the link between boiling and epithermal Ag-Au mineralization in the La Luz area, Guanajuato mining district, Mexico: Ore Geology Reviews, v. 89, p. 143–170.

Monecke, T., Monecke, J., Reynolds, T.J., Tsuruoka, S., Bennett, M. N., Skewes, W. B., and Palin, R. M., 2018, Quartz solubility in the H_2O-NaCl system: A framework for understanding vein formation in porphyry copper deposits: Economic Geology, v. 113, p. 1007–1046.

Moore, W.J., and Nash, J.T., 1974, Alteration and fluid inclusion studies of the porphyry copper ore body at Bingham, Utah: Economic Geology, v. 69, p. 631–645.

Müller, A., Herrington, R., Armstrong, R., Seltman, R., Kirwin, D.J., Stenina, N.G., and Kronz, A., 2010, Trace elements and cathodoluminescence of quartz in stockwork veins of Mongolian porphyry-style deposits: Mineralium Deposita, v. 45, p. 707–727.

Norton, D., 1978, Sourcelines, sourceregions, and pathlines for fluids in hydrothermal systems related to cooling plutons: Economic Geology, v. 73, p. 21–28.

Oakes, C.S., Bodnar, R.J., Simonson, J.M., and Pitzer, K.S., 1994, Critical and supercritical properties for 0.3 to 3.0 mol·kg^{-1} $CaCl_{2(aq)}$: Geochimica et Cosmochimica Acta, v. 58, p. 2421–2431.

Paradis, S., Chi, G., and Lavoie, D., 2004, Fluid inclusion and isotope evidence for the origin of the Upton Ba-Zn-Pb deposit, Quebec Appalachians, Canada: Economic Geology, v. 99, p. 807–817.

Pelch, M.A., Appold, M.S., Emsbo, P., and Bodnar, R.J., 2015, Constraints from fluid inclusion compositions on the origin of Mississippi Valley-type mineralization in the Illinois-Kentucky district: Economic Geology, v. 110, p. 787–808.

Pudack, C., Halter, W.E., Heinrich, C.A., and Pettke, T., 2009, Evolution of magmatic vapor to gold-rich epithermal liquid: The porphyry to epithermal transition at Nevados de Famatina, northwest Argentina: Economic Geology, v. 104, p. 449–477.

Ramsay, J.G., 1980, The crack-seal mechanism of rock deformation: Nature, v. 284, p. 135–139.

Redmond, P.B., Einaudi, M.T., Inan, E.E., Landtwing, M.R., and Heinrich, C.A., 2004, Copper deposition by fluid cooling in intrusion-centered systems: New insight from the Bingham porphyry ore deposit, Utah: Geology, v. 32, p. 217–220.

Reynolds, B.A., Matty, D.J., Jackson, J.L., Chandonais, D.R., and Student, J.J., 2007, Petrology and geochemistry of the Joshua Flat quartz monzonite, White-Inyo Mountains, California: Geological Society of America Abstracts with Program, v. 39, p. 318.

Reynolds, T.J., and Beane, R.E., 1985, Evolution of hydrothermal fluid characteristics at the Santa Rita, New Mexico, porphyry copper deposit: Economic Geology, v. 80, p. 1328–1347.

Richardson, C.K., and Pinckney, D.M., 1984, The chemical and thermal evolution of the fluids in the Cave-in-Rock fluorspar district, Illinois: Mineralogy, paragenesis, and fluid inclusions: Economic Geology, v. 79, p. 1833–1856.

Richardson, C.K., Rye, R.O., and Wasserman, M.D., 1988, The chemical and thermal evolution of the fluids in the Cave-in-Rock fluorspar district, Illinois: Stable isotope systematics at the Deardorff mine: Economic Geology, v. 83, p. 765–783.

Rimstidt, J.D., 1997, Gangue mineral transport and deposition, *in* Barnes, H.L., ed., Geochemistry of hydrothermal ore deposits: New York, Wiley, p. 487–515.

Robert, F., Boullier, A.-M., and Firdaous, K., 1995, Gold-quartz veins in metamorphic terranes and their bearing on the role of fluids in faulting: Journal of Geophysical Research, v. 100, p. 12,861–12,879.

Roedder, E., 1962, Ancient fluids in crystals: Scientific American, v. 207, p. 38–47.

——1971, Fluid inclusion studies on the porphyry-type ore deposits at Bingham, Utah, Butte, Montana, and Climax, Colorado: Economic Geology, v. 66, p. 98-120.

——1974, Changes in ore fluid with time, from fluid inclusion studies at Creede, Colorado: International Association on the Genesis of Ore

Deposits (IAGOD) Symposium, 4th, Varna, Bulgaria, 1974, Proceedings, v. 2, p. 179–185.
——1984, Fluid inclusions: Mineralogical Society of America, Reviews in Mineralogy, v. 12, 646 p.
Schmidt, C., and Bodnar, R.J., 2000, Synthetic fluid inclusions: XVI. PVTX properties in the system H_2O-NaCl-CO_2 at elevated temperatures, pressures, and salinities: Geochimica et Cosmochimica Acta, v. 64, p. 3853–3869.
Schmidt, C., Rosso, K.M., and Bodnar, R.J., 1995, Synthetic fluid inclusions. XIII: Experimental determination of the PVTX properties in the system (H_2O + 40 wt % NaCl)-CO_2 at elevated temperatures and pressures: Geochimica et Cosmochimica Acta, v. 59, p. 3953–3959.
Seedorff, E., Dilles, J.H., Proffett Jr., J.M., Einaudi, M.T., Zurcher, L., Stavast, W.J., Johnson, D.A., and Barton, M.D., 2005, Porphyry deposits: Characteristics and origin of hypogene features: Economic Geology 100th Anniversary Volume, p. 251–298.
Shamanian, G.H., Hedenquist, J.W., Hattori, K.H., and Hassanzadeh, J., 2004, The Gandy and Abolhassani epithermal prospects in the Alborz magmatic arc, Semnan Province, northern Iran: Economic Geology, v. 99, p. 691–712.
Simeone, R., and Simmons, S.F., 1999, Mineralogical and fluid inclusion studies of low-sulfidation epithermal veins at Osilo (Sardinia), Italy: Mineralium Deposita, v. 34, p. 705–717.
Simmons, S.F., Gemmel, J.B., and Sawkins, F.J., 1988, The Santo Niño silver-lead-zinc vein, Fresnillo district, Zacatecas, Mexico: Part II. Physical and chemical nature of ore-forming solutions: Economic Geology, v. 83, p. 1619–1641.
Simmons, S.F., White, N.C., and John, D.A., 2005, Geological characteristics of epithermal precious and base metal deposits: Economic Geology, v. 100, p. 485–522.
Simmons, W.B., and Webber, K.L., 2008, Pegmatite genesis: State of the art: European Journal of Mineralogy, v. 20, p. 421–438.
Simpson, M.P., and Mauk, J.L., 2011, Hydrothermal alteration and veins at the epithermal Au-Ag deposits and prospects of the Waitekauri area, Hauraki Goldfield, New Zealand: Economic Geology, v. 106, p. 945–973.
Simpson, M.P., Strmic Palinkas, S., Mauk, J.L., and Bodnar, R.J., 2015, Fluid inclusions chemistry of adularia-sericite epithermal Au-Ag deposits of the southern Hauraki Goldfield, New Zealand: Economic Geology, v. 110, p. 763–786.
Smith, D.L., and Evans, B., 1984, Diffusional crack healing in quartz: Journal of Geophysical Research, v. 89, p. 4125–4135.
Spencer, E., Wilkinson, J.J., Creaser, R.A., and Seguel, J., 2015, The distribution and timing of molybdenite mineralization at the El Teniente Cu-Mo porphyry deposit, Chile: Economic Geology, v. 110, p. 387–421.
Spry, P.G., and Fuhrmann, G.D., 1994, Additional fluid inclusion data for the Illinois-Kentucky fluorspar district: Evidence for the lack of regional thermal gradient: Economic Geology, v. 89, p. 288–306.
Spry, P.G., Koellner, M.S., Richardson, C.K., and Jones, H.D., 1990, Thermochemical changes in the ore fluid during deposition at the Denton mine, Cave-in-Rock fluorspar district, Illinois: Economic Geology, v. 85, p. 172–181.
Steele-MacInnis, M., Lecumberri-Sanchez, P., and Bodnar, R.J., 2015, Synthetic fluid inclusions XX. Critical PTx properties of H_2O-$FeCl_2$ fluids: Geochimica et Cosmochimica Acta, v. 148, p. 50–61.
Sterner, S.M., and Bodnar, R.J., 1984, Synthetic fluid inclusions in natural quartz I. Compositional types synthesized and applications to experimental geochemistry: Geochimica et Cosmochimica Acta, v. 48, p. 2659–2668.
Steven, T.A., and Eaton, G.P., 1975, Environment of ore deposition in the Creede mining district, San Juan Mountains, Colorado: I. Geologic, hydrologic, and geophysical setting: Economic Geology, v. 70, p. 1023–1037.
Stowell, J.F.W., Watson, A.P., and Hudson, N.C., 1999, Geometry and population systematics of a quartz vein set, Holy Island, Anglesey, North Wales: Geological Society of London Special Publications, v. 155, p. 17–33.
Straathof, L.L., Matty, D.J., and Student, J.J., 2006, Petrology and geochemistry of the EJB diorite, White-Inyo Mountains, eastern California: Geological Society of America Abstracts with Program, v. 38, p. 353.
Teinturier, S., and Pironon, J., 2003, Synthetic fluid inclusions as recorders of microfracture healing and overgrowth formation rates: American Mineralogist, v. 88, p. 1204–1208.
Touret, J.L.R., 1981, Fluid inclusions in high-grade metamorphic rocks: Mineralogical Association of Canada Short Course, v. 6, p. 182–208.
Ulrich, M.R., and Bodnar, R.J., 1988, Systematics of fluid inclusions stretching II: Barite at 1 atm confining pressure: Economic Geology, v. 83, p. 1037–1046.
Van den Kerkhof, A.M., and Hein, U.F., 2001, Fluid inclusion petrography: Lithos, v. 55, p. 27–47.
Vidal, C.P., Guido, D.M., Jovic, S.M., Bodnar, R.J., Moncada, D., Melgarejo, J.C., and Hames, W., 2016, The Marianas-San Marcos vein system: Characteristics of a shallow Au-Ag low-sulfidation deposit at Cerro Negro district, Deseado massif, Patagonia, Argentina: Mineralium Deposita, v. 51, p.725–748.
Vityk, M.O., and Bodnar, R.J., 1995, Do fluid inclusions in high-grade metamorphic terranes preserve peak metamorphic density during retrograde decompression?: American Mineralogist, v. 80, p. 641–644.
Vityk, M.O., Bodnar, R.J., and Schmidt, C.S., 1994, Fluid inclusions as tectonothermobarometers: Relation between pressure-temperature history and reequilibration morphology during crustal thickening: Geology, v. 22, p. 731–734.
Vityk, M.O., Bodnar, R.J., and Doukhan, J.-C., 2000, Synthetic fluid inclusions. XV. TEM investigation of plastic flow associated with reequilibration of fluid inclusions in natural quartz: Contributions to Mineralogy and Petrology, v. 139, p. 285–297.
Wallier, S., Rey, R., Kouzmanov, K., Pettke, T., Heinrich, C.A., Leary, S., O'Connor, G., Tămaş, C.G., Vennemann, T., and Ullrich, T., 2006, Magmatic fluids in the breccia-hosted epithermal Au-Ag deposit of Roşia Montană, Romania: Economic Geology, v. 101, p. 923–954.
Watson, A.P., 1999, The timing and significance of quartz veins in greenschist facies metamorphic rocks with particular reference to the Precambrian of Holy Island, Anglesey, Wales: Ph.D. dissertation, Derby, United Kingdom, University of Derby, 235 p.
Weis, P., Dreisner, T., and Heinrich, C.A., 2012, Porphyry-copper ore shells form at stable pressure-temperature fronts within dynamic plumes: Science, v. 338, 1613–1616.
Werre Jr., R.W., Bodnar, R.J., Bethke, P.M., and Barton, P.B., 1979, A novel gas-flow fluid inclusion heating/freezing stage: Geological Society of America Abstracts with Program, v. 11, p. 539.
Woods, T.L., Roedder, E., and Bethke, P.M., 1982, Fluid inclusion data on samples from Creede, Colorado, in relation to mineral paragenesis: U.S. Geological Survey Open-File Report 82–313, 7 p.

András Fall is a research associate at the Bureau of Economic Geology at the University of Texas at Austin. He has a B.Sc. degree from the Babeş-Bolyai University in Cluj-Napoca, Romania, and M.Sc. and Ph.D. degrees from Virginia Tech, Blacksburg, Virginia. His research focuses on fundamental and applied problems related to structural diagenesis and fluid inclusion research by studying the interaction of geochemical and mechanical processes in sedimentary rocks and the properties and role of fluids in diagenetic processes. He combines geochemistry and fracture analysis to study fracture formation and cementation mechanisms, fracture timing, and pore-fluid pressure-temperature-composition evolution in fractured reservoirs.

Bob Bodnar is a University Distinguished Professor and C.C. Garvin Professor of Geochemistry at the Department of Geosciences at Virginia Tech, Blacksburg, Virginia. He received a B.Sc. degree from the University of Pittsburgh, Pennsylvania, an M.Sc. degree from the University of Arizona, and a Ph.D. degree in geochemistry and mineralogy from Pennsylvania State University. His research involves the distribution, properties, and role of fluids in Earth and planetary systems through field, laboratory, analytical, experimental, and theoretical studies of fluid inclusions in ore deposits and other geologic environments.